

NAVAL POSTGRADUATE SCHOOL Monterey, California



THESIS

STEPPED FREQUENCY IMAGING RADAR SIMULATION

by

Mun, Kok Leong

March 2000

Thesis Advisor:
Second Reader:

David C. Jenn
Jeffrey B. Knorr

Approved for public release; distribution is unlimited.

REPORT DOCUMENTATION PAGE

Form Approved
OMB No. 0704-0188

Public reporting burden for this collection of information is estimated to average 1 hour per response, including the time for reviewing instruction, searching existing data sources, gathering and maintaining the data needed, and completing and reviewing the collection of information. Send comments regarding this burden estimate or any other aspect of this collection of information, including suggestions for reducing this burden, to Washington headquarters Services, Directorate for Information Operations and Reports, 1215 Jefferson Davis Highway, Suite 1204, Arlington, VA 22202-4302, and to the Office of Management and Budget, Paperwork Reduction Project (0704-0188) Washington DC 20503.

1. AGENCY USE ONLY (Leave blank)		2. REPORT DATE March 2000	3. REPORT TYPE AND DATES COVERED Master's Thesis	
4. TITLE AND SUBTITLE Stepped Frequency Imaging Radar Simulation			5. FUNDING NUMBERS	
6. AUTHOR(S) Mun, Kok Leong				
7. PERFORMING ORGANIZATION NAME(S) AND ADDRESS(ES) Naval Postgraduate School Monterey, CA 93943-5000			8. PERFORMING ORGANIZATION REPORT NUMBER	
9. SPONSORING / MONITORING AGENCY NAME(S) AND ADDRESS(ES)			10. SPONSORING / MONITORING AGENCY REPORT NUMBER	
11. SUPPLEMENTARY NOTES The views expressed in this thesis are those of the author and do not reflect the official policy or position of the Department of Defense or the U.S. Government.				
12a. DISTRIBUTION / AVAILABILITY STATEMENT Approved for public release; distribution is unlimited.			12b. DISTRIBUTION CODE	
<p>ABSTRACT (maximum 200 words) In this thesis, a technique involving Stepped Frequency and Inverse Synthetic Aperture Radar (ISAR) processing have been employed to develop two-dimensional radar images of an aircraft target. Radar returns from prominent scatterers of various parts of the target will be processed and displayed. The processing is a combination of two high-resolution processes: development of a high-range resolution (HRR) profile in slant range using the stepped frequency waveform, and the development of a high-resolution profile in cross-range using the ISAR technique. With these two techniques complementing each other, images of targets' dominant scatterers can be extracted, processed and displayed. With intelligence databases built over time, precise recognition of target type can be identified.</p>				
14. SUBJECT TERMS Stepped Frequency Waveform, Inverse Synthetic Aperture Radar (ISAR) Processing, High Range Resolution Profile (HRR)			15. NUMBER OF PAGES 75	
			16. PRICE CODE	
17. SECURITY CLASSIFICATION OF REPORT Unclassified	18. SECURITY CLASSIFICATION OF THIS PAGE Unclassified	19. SECURITY CLASSIFICATION OF ABSTRACT Unclassified	20. LIMITATION OF ABSTRACT UL	

THIS PAGE INTENTIONALLY LEFT BLANK

Approved for public release; distribution is unlimited

STEPPED FREQUENCY IMAGING RADAR SIMULATION

Mun, Kok Leong
Singapore, Ministry of Defense
B.Eng.(Elect.), National University of Singapore, 1991

Submitted in partial fulfillment of the
requirements for the degree of

MASTER OF SCIENCE IN ELECTRICAL ENGINEERING

From the

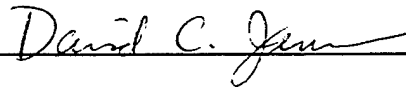
**NAVAL POSGRADUATE SCHOOL
March 2000**

Author:

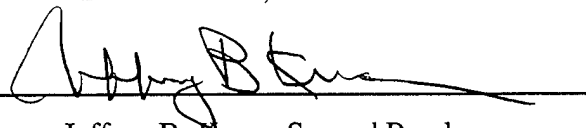


Mun, Kok Leong

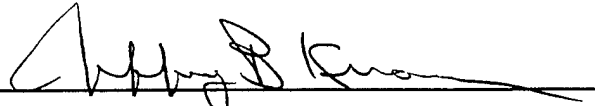
Approved by:



David C. Jenn, Thesis Advisor



Jeffrey B. Knorr, Second Reader



Jeffrey B. Knorr, Chairman
Department of Electrical and Computer Engineering

THIS PAGE INTENTIONALLY LEFT BLANK

ABSTRACT

In this thesis, a technique involving Stepped Frequency and Inverse Synthetic Aperture Radar (ISAR) processing have been employed to develop two-dimensional radar images of an aircraft target. Radar returns from prominent scatterers of various parts of the target are processed and displayed. The processing is a combination of two high-resolution techniques: development of a high-range resolution (HRR) profile in slant range using the stepped frequency waveform, and the development of a high-resolution profile in cross-range using the ISAR technique. With these two techniques complementing each other, images of targets' dominant scatterers can be extracted, processed and displayed. With intelligence databases built over time, precise recognition of target type can be achieved.

THIS PAGE INTENTIONALLY LEFT BLANK

TABLE OF CONTENTS

I.	INTRODUCTION	1
	A. BACKGROUND	1
	B. OBJECTIVE	1
	C. RELATED WORK	1
	D. ORGANIZATION	3
II.	STEPPED FREQUENCY PRINCIPLES	5
	A. BLOCK DIAGRAM	5
	B. WAVEFORM	7
	C. KEY PARAMETERS	11
	1. <i>Instantaneous and Effective Bandwidth</i>	11
	2. <i>Downrange Resolution</i>	12
	3. <i>Downrange Ambiguities</i>	13
	4. <i>Product $\tau\Delta f$</i>	15
	5. <i>Selection of Frequency Step Size</i>	16
III.	INVERSE SYNTHETIC ARRAY RADA (ISAR) PROCESSING	19
	A. ISAR THEORY	19
	B. ISAR CROSSRANGE CALCULATION	19
	C. MAXIMUM UNFOCUSSED INTEGRATION ANGLE	22
	D. CROSSRANGE SAMPLING CRITERIA	23
IV.	RANGE DOPPLER PROCESSING	25
	A. UNAMBIGUOUS WINDOW AND RESOLUTION	25
	B. FAST FOURIER TRANSFORM	26
	C. TARGET RADIAL (TRANSLATIONAL) VELOCITY EFFECTS	28

1. <i>Range Offset</i>	28
2. <i>Range Walk</i>	29
D. TARGET ANGULAR VELOCITY EFFECTS.....		29
1. <i>Range-Doppler Interaction</i>	29
2. <i>Cell Migration</i>	30
V. SIMULATION DESIGN	31
A. APPROACH	31
B. TARGET	32
C. RADAR AND TARGET PARAMETERS	35
D. STEPPED FREQUENCY PROCESSING PARAMETERS AND REQUIREMENTS	35
E. ISAR PROCESSING PARAMETERS & REQUIREMENTS	36
VI. SIMULATION RESULTS AND DISCUSSION	37
A. BANDWIDTH OF STEPPED FREQUENCY WAVEFORM	37
B. TRACKING WINDOW AND EFFECTS OF TARGET ANGULAR VELOCITY	40
1. <i>Scenario 1</i>	42
2. <i>Scenario 2</i>	44
C. IMAGE OF SIMPLE TARGET	47
D. IMAGE OF COMPLEX TARGET	49
VII. CONCLUSIONS AND RECOMMENDATIONS	51
APPENDIX A – STEPPED FREQUENCY WAVEFORM PROGRAM CODES	53
APPENDIX B – STEPPED FREQUENCY AND ISAR PROCESSING PROGRAM CODES	55
LIST OF REFERENCES	63

INITIAL DISTRIBUTION LIST65

I. INTRODUCTION

A. BACKGROUND

Since the 1990s, radar imaging and multi-dimensional radar systems have become widely used in many areas, both military and commercial. This came about due to the advent of more advanced waveform generation and signal processing techniques. The requirement for high resolution radars in military applications has always been a top priority in radar system design. However, there is a fundamental tradeoff between resolution and the radar system's bandwidth. The wide bandwidth required for high resolution is difficult to achieve. The stepped frequency waveform is an alternative to building wide bandwidth devices.

Essentially, the stepped frequency radar employs inter-pulse pulse compression, in which the carrier frequency of successive pulses is changed by a fixed frequency step, Δf . Due to this technique, a wide bandwidth is inherently achieved over several pulses instead of within a single pulse. However, its instantaneous bandwidth remains small, and this feature is important because of the simpler hardware involved in the receiver for a smaller instantaneous bandwidth. The effective stepped frequency waveform (SFWF) bandwidth is the product of the number of coherently integrated pulses, N , and the frequency step size, Δf .

The returns of the N pulses at different carrier frequencies form the frequency spectrum of the target reflectivity and are coherently integrated by the inverse fast Fourier Transform (IFFT) to give the high resolution range (HRR) profile. The HRR

profile does not give the absolute range position of the target but gives the relative position of each scatterer within the conventional range bin.

The key advantage of the stepped frequency implementation as compared to other pulse compression techniques is its high range resolution (on the order of a fraction of a meter is achievable) without compromising its instantaneous bandwidth, or target detection range. It is easily implemented by adding a frequency synthesizer to a conventional narrowband receiver and performing the necessary signal processing on the received signal.

The two main limitations of the stepped frequency radar implementation are as follows:

- a. The stepped frequency radar cannot directly measure the velocity of moving targets based on the doppler shift. This is due to the frequency shift in the carrier during transmission.
- b. The stepped frequency implementation requires additional time to transmit and receive N pulses.

Inverse Synthetic Aperture Radar (ISAR) is used to image targets in the cross-range dimension due to their rotational motion. The ISAR, like the SFWF, works on the principle of doppler shifts due to target rotation, which causes a scatterer on the target to change its relative position from the radar over time. It can be seen that a scatterer located in the center of the rotating platform will therefore experience no doppler shifts, hence registering zero frequency shift over time. However, this processing requires the phase of the transmitted pulse be almost constant over the processing interval for the Range Rate Interval (RRI), which is the duration of the stepped frequency waveform.

Both of the above techniques are also termed as multiple pulse processes. The ISAR technique requires a fixed frequency measurement of a non-stationary target and the SFWF requires a sweep frequency measurement of a stationary target. Proper selection of the radar parameters can yield a radar design for optimum range resolutions in both down-range and cross-range for a particular target of interest, especially so for radars with adaptive operating parameters.

B. OBJECTIVE

The objective of this thesis is to use two proven high resolution processing techniques, namely stepped frequency and ISAR processing, to image the simulated signal returns from multiple scatterers on an object. Applications include imaging for target identification and radar cross section (RCS) measurements. RCS measurement and reduction are the primary applications of interest in this research. Unlike the general imaging case in which the target and radar geometrical relationships are often non-optimum, the measurement application allows the target motion to be controlled precisely. The resulting images can isolate individual scattering sources on a target. Knowledge of the individual scatterer's characteristics permits the development of a RCS reduction strategy.

C. RELATED WORK

The theory of stepped frequency has been explored in two previous theses [1,2]. In [1], various radial velocity compensation techniques were explored to eliminate the image spreading and shifting effects, while in [2], the effects of changing the various

radar parameters on the stepped frequency performance were studied. This thesis goes one step further, in that, the stepped frequency processing is combined with the ISAR processing to form images from the signal returns of targets [3].

D. ORGANIZATION

This thesis starts out with an introduction of the two high resolution processing techniques. Chapter II reviews the stepped frequency principles [4] and Chapter III reviews the ISAR processing technique [4,5]. The considerations for selection of the various radar parameters to obtain the required radar performances in detecting and imaging an aircraft target are also covered in these two chapters. Chapter IV combines these two techniques in the generation of a range-doppler profile using the Fast Fourier Transform (FFT) and discusses the effects of the target's radial and angular motion on the processed target image, which results in an optimal tracking window for the selected radar parameters. This is followed by the design of the radar parameters to detect a 15 m aircraft target and the simulation of the aircraft image (both a simple and complex aircraft) in Chapters V and VI respectively. Chapter VI also shows the simulated effects of range walk and range spread on the image of each scatterer when the radar conditions for the optimal tracking window are not met. Chapter VII presents the conclusions and suggestions for future work.

II. STEPPED FREQUENCY PRINCIPLES

A. Block Diagram

The hardware implementation of the stepped frequency radar is shown in Figure 2.1. The coherent stepped frequency synthesizer generates an output which is stepped in frequency from pulse to pulse by a fixed frequency step size.

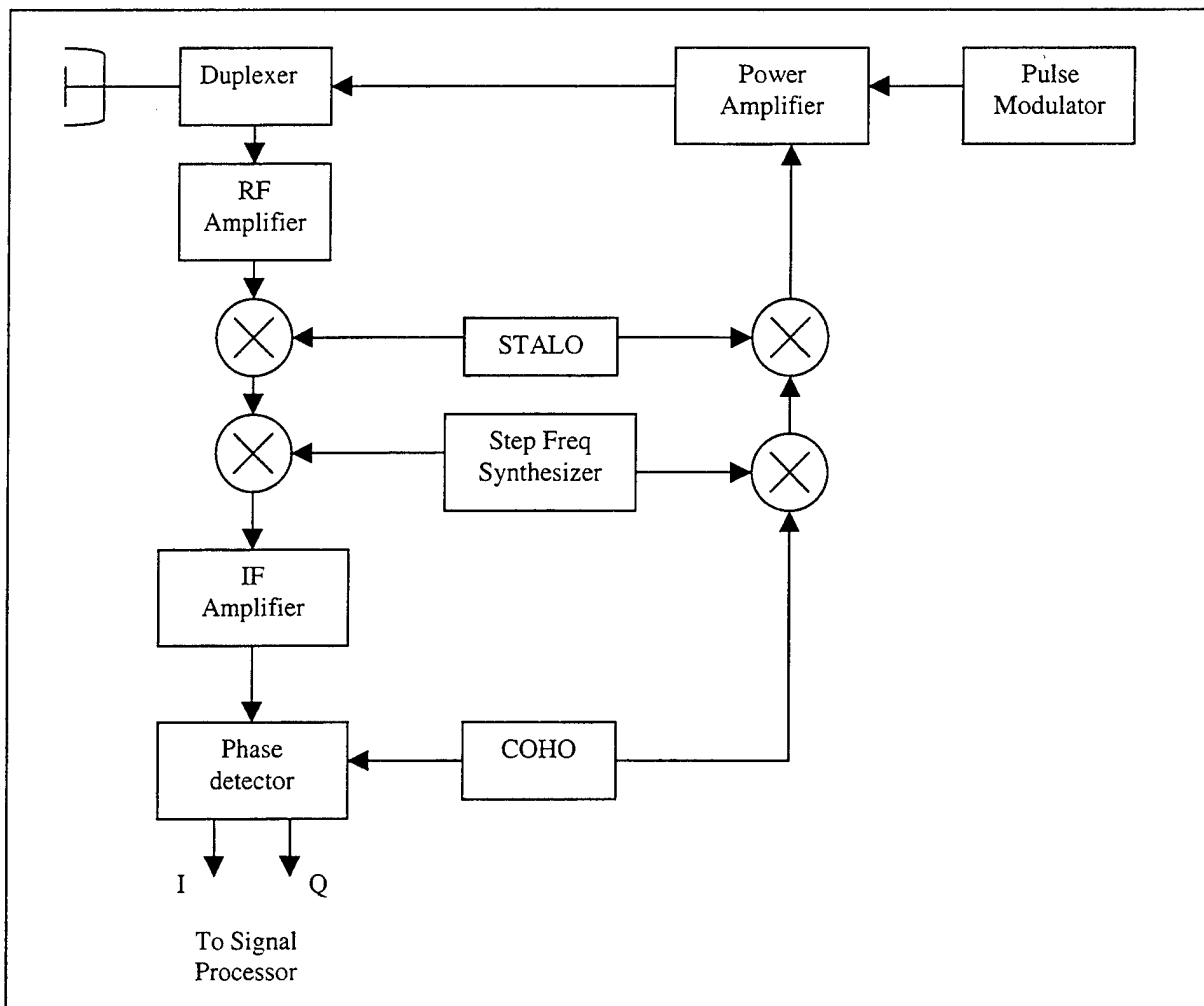


Figure 2.1 Block Diagram of Step Frequency Radar Receiver.

On the transmitter side, the output of the coherent oscillator (COHO) is mixed with the output of the stepped frequency synthesizer (up-conversion). The sum of these two frequencies is up-converted to the final transmitted frequency after mixing with the stable local oscillator (STALO). The frequency is then pulse-modulated and power amplified before transmission into space.

The frequency of each transmitted pulse is comprised of three components: the fixed intermediate frequency of the coherent oscillator, fixed radio frequency of the local oscillator and the variable frequency of the stepped frequency synthesizer.

On the receiver side, the return radio-frequency target signal is amplified and down-converted by first mixing it with the output of the stable local oscillator. The resulting signal is further down-converted to the intermediate frequency (IF) by mixing it with the output of the stepped frequency synthesizer.

The stepped frequency synthesizer is synchronized with the transmitter to allow the transmitted carrier frequency and the output of the stepped frequency synthesizer to use the same stepped frequency in the same pulse repetition interval. This permits the multiple-time-around clutter to be filtered out, as it will lie outside the passband of the intermediate frequency amplifier.

The output signal obtained after the second mixing is the intermediate-frequency signal which is fed into the coherent phase detector through an intermediate-frequency amplifier with a bandwidth approximately equal to the inverse of the pulse width, centered on the frequency of the coherent oscillator.

B. Waveform

The stepped frequency waveform is the interpulse version of the pulse compression technique employed in conventional high resolution radars. A sequence of N pulses at a fixed pulse repetition frequency (PRF) but different carrier frequency is transmitted by the stepped frequency radar. Each set of N pulses is called a coherent processing interval. Figure 2.2 shows a stepped frequency waveform, and Figure 2.3 shows its corresponding frequency spectrum. Note that the frequency of each pulse in the sequence is linearly increased from pulse to pulse by a fixed increment, with the frequency of the first pulse being the nominal carrier frequency, f_0 , and the subsequent pulses having a difference of Δf (frequency step size) from the preceding pulse. Thus, for the n -th transmitted pulse in the sequence, with $n=0,1,2, \dots,N-1$, the carrier frequency is given by

$$f_n = f_0 + n\Delta f. \quad (2.1)$$

If the transmitted pulsed signal for the n -th pulse is

$$s_1(t) = A_1 \cos[2\pi(f_0 + n\Delta f)t], \quad (2.2)$$

then the target signal received after a time delay of $2R/c$ for a target range of R is given by

$$s_2(t) = A_2 \cos[2\pi(f_0 + n\Delta f)(t-2R/c)], \quad (2.3)$$

where c is the speed of light.

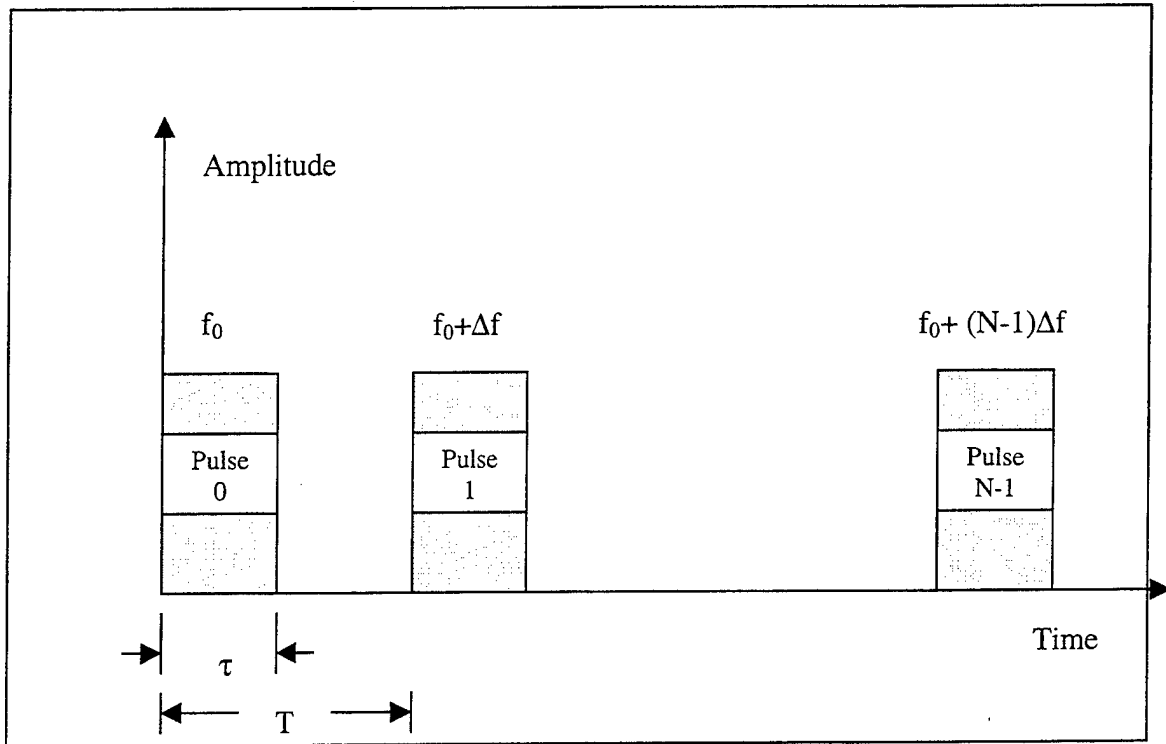


Figure 2.2 Pulse Sequence of Step Frequency Waveform.

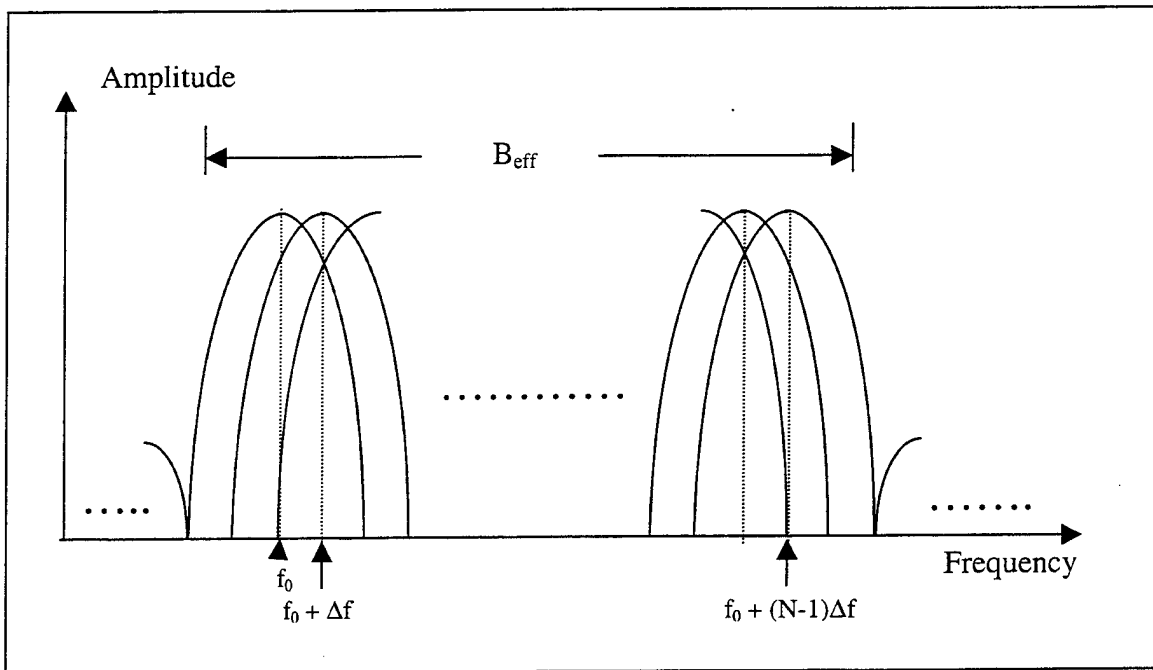


Figure 2.3 Frequency Spectrum of Step Frequency Waveform.

The output from the coherent phase detector is modeled as the product of the received signal with the reference signal followed by a lowpass filter. The output of the mixer of the coherent phase detector is

$$\begin{aligned}
 s_1(t)s_2(t) &= A_1A_2\cos[2\pi(f_0 + n\Delta f)t] \cos[2\pi(f_0 + n\Delta f)(t - \frac{2R}{c})] \\
 &= \frac{A_1A_2}{2} \{ \cos[2\pi(f_0 + n\Delta f)t - 2\pi(f_0 + n\Delta f)(t - \frac{2R}{c})] + \cos[2\pi(f_0 + n\Delta f)\frac{2R}{c}] \}.
 \end{aligned}
 \tag{2.4}$$

The first component of Equation 2.4, which is the high frequency term, is filtered out by the low-pass filter. Therefore, the output of the coherent phase detector is

$$\begin{aligned}
 s(t) &= \frac{A_1A_2}{2} \cos[2\pi(f_0 + n\Delta f)\frac{2R}{c}] \\
 &\equiv A\cos[2\pi(f_0 + n\Delta f)\frac{2R}{c}].
 \end{aligned}
 \tag{2.5}$$

The output of the in-phase and quadrature (I-Q) detector can be represented as

$$s(t) = Ae^{-j\phi_n} = I_i + jQ_i, \tag{2.6}$$

where $\phi_n = 2\pi(f_0 + n\Delta f)\frac{2R}{c}$.

If the target moves with a constant radial velocity, v , the range changes with each pulse as

$$R_n = R_0 + vnT, \quad (2.7)$$

where T is the pulse repetition interval (PRI) of the sequence of pulses in seconds. From Equations 2.6 and 2.7, the phase can be simplified to

$$\phi_n = 2\pi(f_0 + n\Delta f)2(R_0 + vnT)/c, \quad (2.8)$$

or when expanded out,

$$\phi_n = \frac{4\pi f_0 R_0}{c} + \frac{4\pi \Delta f R_0 (n-1)T}{Tc} - \frac{4\pi v f_0 (n-1)T}{c} - \frac{4\pi \Delta f v (n-1)^2 T^2}{Tc}. \quad (2.9)$$

\Downarrow
 1st term

\Downarrow
 2nd term

\Downarrow
 3rd term

\Downarrow
 4th term

The first term represents a constant phase shift and does not figure into the stepped frequency implementation. The second term represents the frequency shift due to the frequency rate of change multiplied by the round-trip delay time. This is also referred to as the induced phase shift. This term gives the desired range resolution of the stepped frequency waveform. The third term of Equation 2.9 gives the doppler frequency due to the radial motion of the target. This component, nevertheless, will add on to the phase component of the 2nd term. It will be interpreted as though there is a range movement of the target. The fourth term in Equation 2.9 is the frequency shift from pulse to pulse and

occurs due to the relative velocity between target and radar. Like the third term, it will result in target spreading in range, attenuation of target amplitude due to the spreading, and shifting (range walking) of the target signal in the range profile. Hence, contributions from the third and fourth terms will corrupt the HRR profile.

C. Key Parameters

The following are the key parameters used in the stepped frequency radar:

1. Instantaneous and Effective Bandwidth

The instantaneous bandwidth of the waveform is the same as that of a single pulse, and is given by the inverse of the pulse width, τ , as

$$B_{\text{inst}} = \frac{1}{\tau}. \quad (2.10)$$

The effective bandwidth is correspondingly given as

$$B_{\text{eff}} = N\Delta f, \quad (2.11)$$

and the design of the stepped frequency waveform is such that

$$B_{\text{eff}} > B_{\text{inst}}. \quad (2.12)$$

2. Downrange Resolution

The downrange (range of target from radar) resolution of a conventional radar is given as:

$$\Delta r_{d,\text{conventional}} = \frac{c\tau}{2}. \quad (2.13)$$

With the stepped frequency implementation, the downrange resolution can be made much smaller, as follows:

$$\Delta r_d = \frac{c}{2B_{\text{eff}}} = \frac{c}{2N\Delta f}. \quad (2.14)$$

From Equation 2.14, the downrange resolution of the stepped frequency waveform can be increased by either increasing the number of pulses in the sequence or the frequency step size. Alternatively, the increase in the downrange resolution can be seen as the original range resolution cell being broken up into N sub-cells. The FFT output of the N samples will generate a high resolution range profile, with resolution

$$\Delta r_d = \frac{R_u}{N} = \frac{c}{2N\Delta f} = \frac{c\tau/2}{N\tau\Delta f}, \quad (2.15)$$

where R_u is the unambiguous range window.

A simplified pictorial representation of $\Delta r_{d,conventional}$, Δr_d , and R_u is given in Figure 2.4. From Equation 2.15, it can be seen that the product of pulse width and frequency step size determines the downrange resolution of the stepped frequency radar.

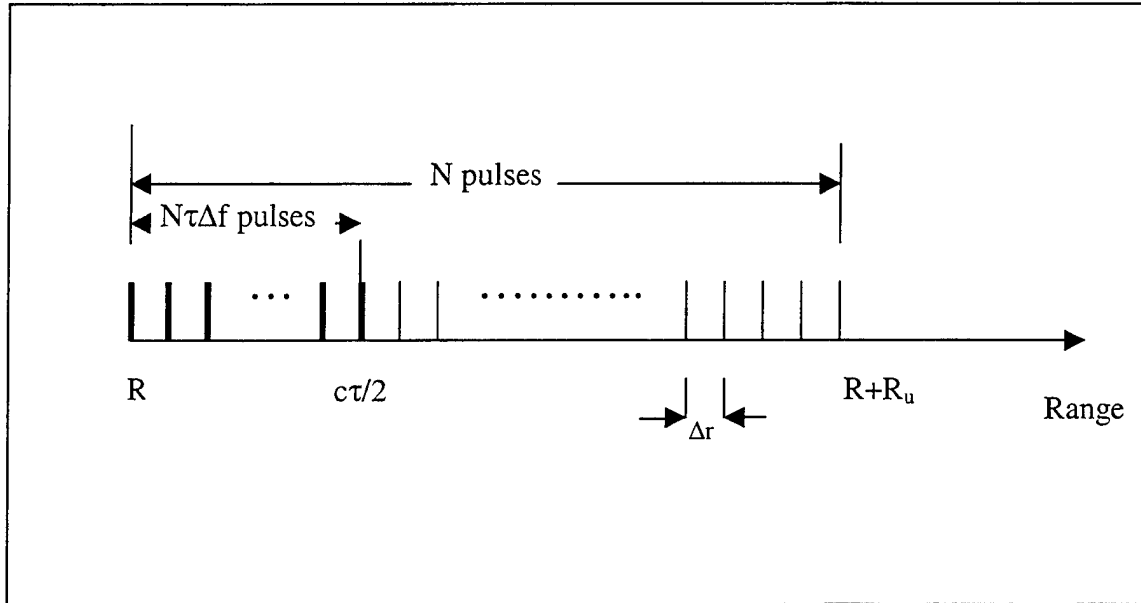


Figure 2.4 Range Resolution with Step Frequency Radar.

3. Downrange Ambiguities

Downrange ambiguities exist for the stepped frequency radar. The maximum unambiguous downrange is associated with the SFWF process and can be determined from the phase ϕ_n of the received echo for frequency step n from a scatterer at range R_0 , given by the 2nd term in the target signal phase Equation 2.9

$$\Phi = 2\pi \frac{\Delta f 2R_0}{T_c} (n-1)T. \quad (2.16)$$

The corresponding frequency shift can be determined from the rate of phase change as

$$f = \frac{\Delta f 2R_0}{T_c} \quad (2.17)$$

By equating the frequency shift to the PRF, f_p

$$f_p = 1/T = \frac{\Delta f 2R_0}{T_c} \quad (2.18)$$

Simplifying, the downrange ambiguity window, R_u , which is equivalent to the maximum downrange image dimension, W_d , gives

$$R_u = \frac{c}{2\Delta f} \quad (2.19)$$

For a frequency step size, Δf , of 10MHz, the unambiguous range window is 15m. Scatterers located at 10m, 25m, 625m will all appear to be at the same range. The stepped frequency processing cannot, therefore, provide absolute range to scatterer, but rather relative range position within the received pulse. The normal time delay measurements (range gating) will have to be used to compute the actual range to the target under range track. Therefore, the range of each scatterer is computed from the combination of information from range gating and relative range from stepped frequency processing. The

absolute range to a scatterer is given as

$$R = R_0 + n \left[\frac{c}{2N\Delta f} \right], \quad (2.20)$$

where R_0 is the absolute range of the scatterer from the beginning of the unambiguous range window. The start range of the unambiguous range window is computed as a integer (n) multiple of $c/2\Delta f$. For example, with $n = 60$, the range gate opens from 900m to 915m. Within that interval, the smallest resolution is given in Equation 2.15.

4. Product $\tau\Delta f$

The high range resolution (HRR) profile of the stepped frequency radar depends to a large extent on the product of the pulse width and frequency step size, $\tau\Delta f$. There are three cases:

- a) $\tau\Delta f = 1$. The unambiguous downrange window, R_u , equals the original range bin size of $c\tau/2$. This represents the minimum required sampling rate in the frequency domain for a given pulse width. The disadvantage of this condition is that the wraparound of scatterer peaks caused by slight changes in the target range is difficult to notice.

- b) $\tau\Delta f < 1$. The original range bin occupies only part of the unambiguous downrange window. This implies oversampling in the frequency domain and will result in a loss in downrange

resolution in the range profile. The advantage of this is that the unused part of the downrange profile serves as a clutter-free zone to detect moving targets.

- c) $\tau\Delta f > 1$. The unambiguous downrange window is smaller than the original range bin. This represents undersampling in the frequency domain. Folding over of targets will result and therefore this condition should be avoided.

5. Selection of Frequency Step Size

The frequency step size is important in determining the size of the ambiguous downrange window and the range resolution under stepped frequency implementation. Generally, the frequency step size is chosen to be approximately half the inverse of the pulse-width [2]. In cases where there are no background scatterers outside the target, like working in an anechoic chamber, the target maximum extent, E , plays a part in influencing the frequency step size, as follows:

$$\Delta f \leq \frac{c}{2E} . \quad (2.21)$$

From the above relationship, the frequency step size varies inversely as the target extent, E . In addition, the pulse width needs to be large enough to encompass the entire

target

$$\tau \geq \frac{2E}{c}. \quad (2.22)$$

Combining Equations 2.18 and 2.19, we obtain the requirement that

$$\Delta f \leq \frac{1}{\tau}. \quad (2.23)$$

THIS PAGE INTENTIONALLY LEFT BLANK

III. INVERSE SYNTHETIC ARRAY RADAR (ISAR) PROCESSING

A. ISAR THEORY

ISAR provides a processing technique capable of high crossrange resolution due to target rotation. This method assumes that velocity compensation has been done to eliminate target-to-radar radial velocity component, which, as explained in the previous chapter, has the effect of range bin shift (or range walk) as well as target spreading within a bin. We recall that the SFWF generates a frequency shift from a known frequency change on a pulse-to-pulse basis. It requires that the target be stationary or velocity-compensated during the RRI. The ISAR processing measures the dominant scatterers' locations on a target arising from a shift in doppler frequency due to changing scatterers' radial velocities as the target rotates.

B. ISAR CROSSRANGE CALCULATION

The crossrange resolution obtained from the ISAR processing is dependent primarily on the doppler shift of the various scatterers located on the target. This is illustrated by Figure 3.1. For this example, there is no translational motion between the radar and the target and therefore the depression angle is zero; that is, all scatterers on the target and the radar are in the same horizontal plane. Also, the target rotates at a constant angular rotation speed of ω rad/s about the axis that is perpendicular to the horizontal plane. From the figure, it can be seen that a point scatterer at a crossrange of r_c from

the center of rotation will have a instantaneous tangential velocity, v , given by

$$v = \omega r. \quad (3.1)$$

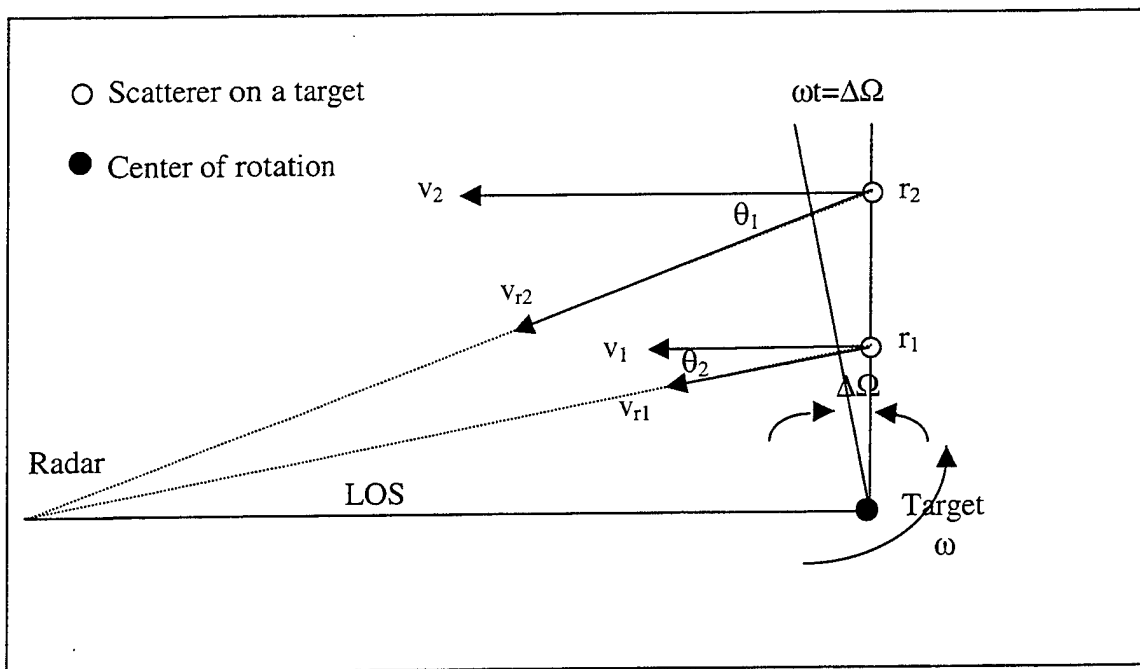


Figure 3.1 ISAR Crossrange Resolution of Two Scatterers.

The corresponding doppler frequency can be computed from

$$f_d = 2\omega r_c \frac{f_c}{c}, \quad (3.2)$$

where f_c is the carrier frequency and c the speed of light at 3×10^8 m/s. For the case of 2 point scatterers located in the same downrange cell, but separated in crossrange by Δr_c ,

the tangential velocity difference is $\omega\Delta r_c$, and the corresponding frequency difference can be computed as

$$\Delta f_c = 2\omega \frac{\Delta r_c f_c}{c} \quad (3.3)$$

The doppler resolution is approximately equal to the reciprocal of the coherent integration time,

$$\Delta f_d = 1/T_i = \frac{1}{M \times \text{PRI}} \quad (3.4)$$

where M is the total number of pulses processed for doppler resolution. For a doppler resolution of Δf_d , the corresponding crossrange resolution is

$$\Delta r_c = \frac{c\Delta f_d}{2\omega f_c} \quad (3.5)$$

and from Equations 3.3, 3.4 and 3.5, we obtain another expression for the crossrange resolution:

$$\Delta r_c = \frac{c}{2\omega T_i f_c} = \frac{\lambda}{2\omega T_i} = \frac{\lambda}{2\psi} \quad (3.6)$$

where λ is the wavelength and ψ the total angle moved during the integration time. As was done for the SFWF, the Fast Fourier transform (FFT) is used to convert the M time samples into a frequency spectrum.

C. MAXIMUM UNFOCUSSED INTEGRATION ANGLE

There is the maximum angle for the target rotation, depending on the target maximum length, whereby phase deviation occurs which causes defocusing of the target image in the crossrange after processing. The defocusing occurs because of the change in distance between the radar and the scatterer as the target rotates. This distance can be converted to an equivalent phase difference. The rule of thumb for the maximum allowable two-way phase deviation before defocusing occurs is given as $\pi/8$ radians [2]. The maximum integration angle before defocusing occurs is

$$\Psi_{\max} = \frac{1}{2} \sqrt{\frac{\lambda}{r}}. \quad (3.7)$$

The maximum target radius, r ($= \frac{E}{2}$ if the center of the target is the center of rotation),

before defocusing occurs, is expressed as

$$r < \frac{2(\Delta r_c)^2}{\lambda}. \quad (3.8)$$

If the criterion for ψ_{\max} is violated, then focusing is required. Essentially, this is done by subtracting or adding the two-way path difference, hence phase difference, as the scatterer rotates around the center of the target.

D. CROSSRANGE SAMPLING CRITERIA

The selection of PRF is determined by the Nyquist sampling requirement to prevent aliasing. Nyquist sampling requires that the signal be sampled at twice the highest expected doppler frequency component. The highest doppler frequency is obtained from the scatterer that is furthest away from the center of rotation, and is given by

$$\text{PRF}_{\text{effective}} = f_{p,\text{effective}} \geq 2f_{d(\max)} = \frac{4f_c}{c} \omega r_{c(\max)}, \quad (3.9)$$

where $r_{c(\max)}$ is the distance of the furthest scatterer from the center of rotation. The effective PRF for a stepped frequency radar can also given be given as

$$\text{PRF}_{\text{effective}} = \text{PRF}/N, \quad (3.10)$$

where N is the number of frequency steps used. This is the unambiguous doppler window. Therefore, the maximum and minimum scatterer doppler frequencies that will not cause aliasing are from $+\text{PRF}_{\text{effective}}/2$ to $-\text{PRF}_{\text{effective}}/2$ Hz. The corresponding unambiguous crossrange window is given as

$$W_c = 2r_{\max} = \frac{c \text{PRF}_{\text{effective}}}{2\omega f_c} = \frac{M\lambda}{2\omega T_i}, \quad (3.11)$$

where T_i is the total coherent integration time for the M ISAR waveforms (fixed frequency time samples).

IV. RANGE-DOPPLER PROCESSING

A. UNAMBIGUOUS WINDOW AND RESOLUTION

The two-dimensional image of a target can be generated from the stepped frequency and ISAR processing. The two image axes are downrange and doppler (crossrange). The downrange and crossrange resolutions are given in Equations 2.15 and 3.6, while the downrange and crossrange windows are given in Equations 2.21 and 3.10, respectively. Both the downrange and doppler (crossrange) windows will combine to give the desired two-dimensional image of a target.

In order to obtain these two dimensions, two transforms are required. For the SFWF, N pulses are transmitted in one waveform and during these N pulses, it is assumed that there is only a very small viewing angle change. For each of the N pulses, a range profile can be generated. Altogether, there are M such range profiles, which can be transformed by a discrete Fourier transform (DFT) to obtain the target doppler information for each range cell. The N pulses and M profiles will therefore define the downrange and crossrange range windows.

Figure 4.1 illustrates the SFWF-ISAR waveform relationship. There are M ($=4$) stepped frequency waveforms, each consisting of N ($=16$) stepped frequency pulses. If the RRI ($= N \times \text{PRI}$) is equal to the dwell time, ie, there is no idle time, then the total integration time T_i is

$$\begin{aligned} T_i &= M \times \text{RRI} \\ &= M \times N \times \text{PRI}. \end{aligned} \tag{4.1}$$

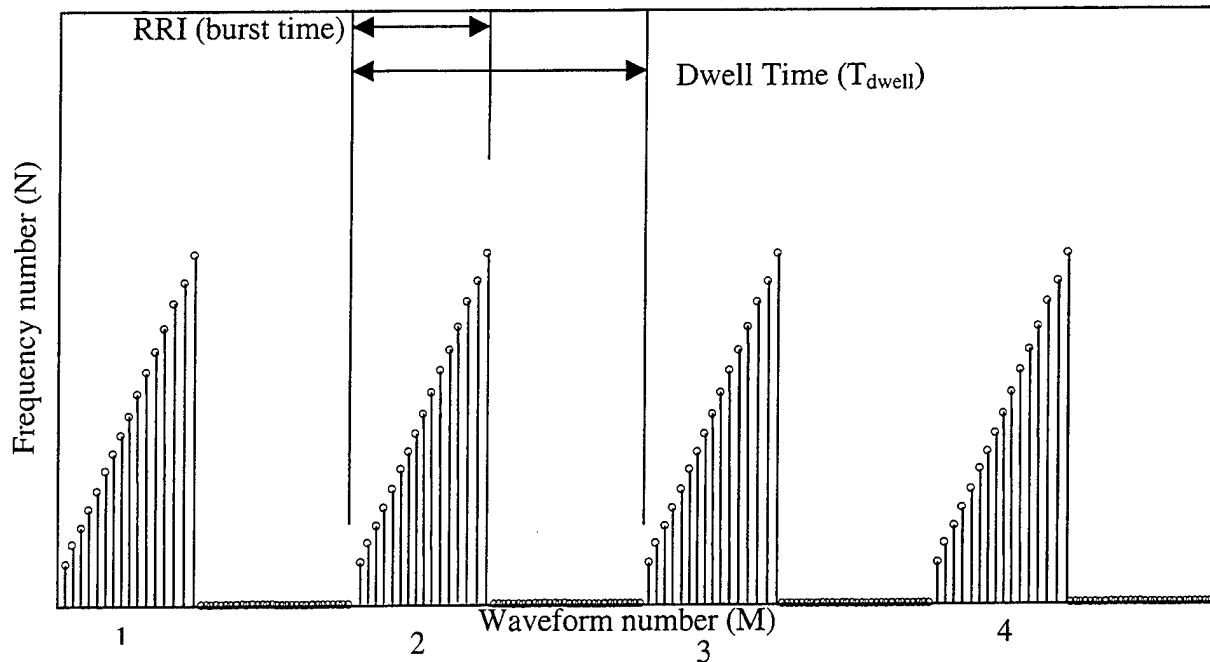


Figure 4.1 Frequencies of Successive Pulses in the SFWF. Each SFWF is Processed to Form One of M HRR Profiles Used In Generating The ISAR Profiles.

B. FAST FOURIER TRANSFORM (FFT)

To illustrate how the FFT is used to generate the two-dimensional image of the target, the returned $M \times N$ data pulses collected are organised into a 2-D array as shown in Figure 4.2. The received frequency signatures of the M bursts are the time history series of the target's reflectivity at each discrete frequency. The radar processor then uses the frequency signatures as the raw data to perform range and doppler processing. For the stepped frequency signals, the range processing performs an N -point 1-D inverse Fourier transform (1-IDFT) for each of the M received frequency signatures. Therefore, M range profiles (ie, the distribution of the target reflectivities in range), each containing N range cells, can be obtained. For each range cell, the M range profiles constitute a new time series, which is sampled at baseband to form M in-phase (I channel) and M quadrature-phase (Q-channel) data.

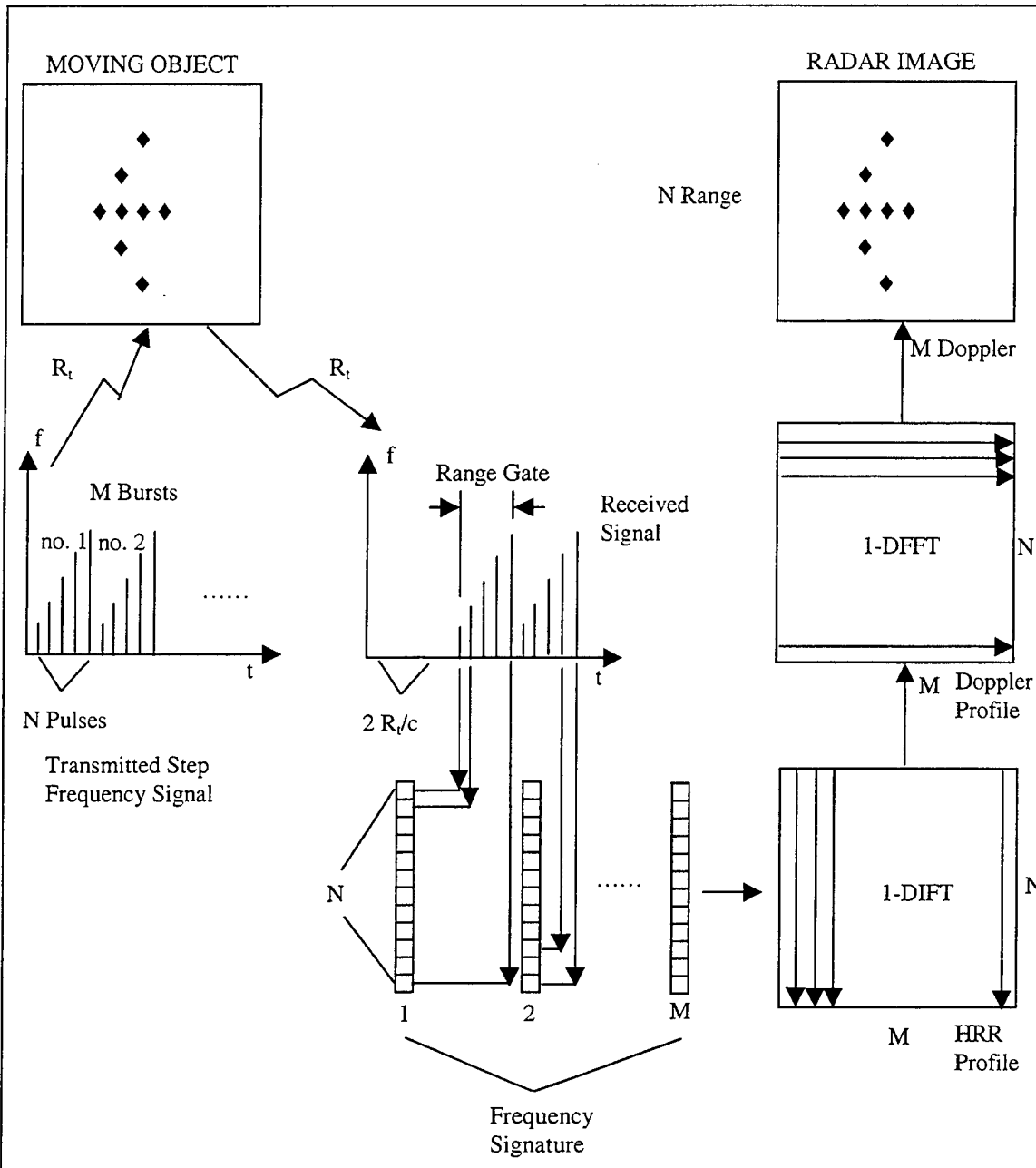


Figure 4.2 Illustration of a Step Frequency ISAR Imaging of a Rotating Target (after [3]).

The 1-D FFT (1-DFFT) is then used for the time history series to generate an M-point doppler spectrum, or doppler profile. Hence, a $N \times M$ image is formed by combining the N doppler spectra at N range cells. Figure 4.2 illustrates the various steps in the processing.

C. TARGET RADIAL (TRANSLATIONAL) VELOCITY EFFECTS

In this thesis, it is assumed that only rotational motion of the aircraft target exists; no translational velocity is modeled or if it is present, is assumed to be compensated. However, for completeness, it is discussed here.

Translational velocity causes the effects described in the following two sections.

1. Range Offset

Also known as range spreading, this causes the range of each scatterer to spread from its actual location to adjacent range cells, thus providing a distorted and undesirable range profile. This spreading needs to be compensated. The formula that relates the range offset or number of bins spread, P, to the radial (translational) velocity is given as follows:

$$P = \frac{v_r NT}{\Delta r} \quad (4.2)$$

where NT = total duration of the stepped frequency waveform, Δr is the effective range resolution, and v_r the radial velocity of target.

2. Range Walk

This has the effect of shifting the range profile by L bins, resulting in an inaccurate position processing of individual scatterers. The formula that relates this range bin shift to the radial velocity is

$$L = \frac{f_c'}{B_{\text{eff}}} P = \frac{f_d N}{f_p}, \quad (4.3)$$

where f_d is the doppler due to uncompensated radial velocity, ie,

$$f_d = \frac{f_c' v_r}{B_{\text{eff}} \Delta r}, \quad (4.4)$$

and f_c' is the nominal transmitter frequency (center frequency)

$$f_c' = f_0 + B_{\text{eff}}. \quad (4.5)$$

D. TARGET ANGULAR VELOCITY EFFECTS

There are two effects due to the rotational motion of the target: (1) range-doppler interaction and (2) cell migration.

1. Range-Doppler Interaction

This will cause range smearing to the range profile. As a rule of thumb [1], in order to avoid range smearing, the rotation angle of the target, ω , should satisfy

$$\omega < \frac{1}{2} \frac{cf_p}{ENf_c} \quad (4.6)$$

The factor of $\frac{1}{2}$ is chosen as a rule of thumb.

2. Cell Migration

Distortion of the range profile occurs due to the quadratic phase variation caused by the circular motion of the scatterers as they rotate. Another way of looking at this is that the radial velocity of the scatterer is not constant throughout the integration time, T_i , during the rotation. When used with the FFT, movement of the scatterers across range cells occur and blurring results. The movement across range cells can occur in both crossrange and downrange.

In order to prevent cell migration from occurring, the selection of radar parameters is important. The occurrence of image blurring can be represented by an indicator, N_d (for downrange) or N_c (for crossrange) as follows:

$$N_{c,d} = \left[\frac{E}{2\Delta r_{c,d}} \right] \left[\frac{c}{f_c} \right] \left[\frac{1}{2\Delta r_{c,d}} \right] \quad (4.7)$$

N_c and N_d represent the number of range bin shifts the image experiences in the crossrange and downrange respectively. To prevent blurring of the image, $N_{c,d}$ should be less than unity. A factor of $\frac{1}{2}$ is used as a rule of thumb. From Equations 2.14, 2.19, 3.6, and 3.11, the values of N_c and N_d determine the optimal crossrange and downrange window. A scatterer located within this window will experience no range bin shifts.

V. SIMULATION DESIGN

A. APPROACH

In this thesis, various point scatterer models of aircraft will be used as the targets from which signals will be received by the radar and processed using stepped frequency and ISAR techniques. Matlab will be used to simulate the target returns and provide the processing tools for the IFFT and DFFT. The approach adopted in the Matlab programming is as follows:

1. The aircraft scatterers are computed in cartesian co-ordinates manually on paper or generated using a Computer-Aided program. The radar is located at the origin.
2. A rotation speed at ω radians per second is selected so that it meets the Nyquist sampling criteria.
3. The various radar parameters are selected and verified to meet both stepped frequency and ISAR processing requirements.
4. The radial velocities, hence doppler frequencies, of the scatterers, as seen by the radar, are computed.
5. Amplitudes for the scatterers are varied according to their orientation to the radar to simulate a realistic target. For example, those scatterers on the leading edge of an aircraft are assigned a higher radar cross section compared to the rest of the scatterers on the trailing edge of the aircraft. This applies only to the complex target.

6. The radar transmits M pulse bursts, each with N pulses, stepped in frequency. It is assumed that, within each burst, the target's doppler is constant. Only the doppler frequency of each of the M bursts changes.
7. The I and Q components of the target returns are generated for each pulse.
8. The I and Q components of the N pulses within each burst are processed using the IFFT to generate the M HRR (downrange information) profiles.
9. The M HRR profiles obtained from step 8 are further processed using the DFFT to generate the Doppler profile. The doppler information is then mapped into crossrange coordinates.
10. The two-dimensional image of the target is mapped using the HRR and doppler profiles.

B. TARGET

A simple wire model of an aircraft with 9 scatterers will be modeled first in order to illustrate the stepped frequency and ISAR processing without having to look at the enormous details arising from a large number of scatterers. The dimensions are as shown in Figure 5.1. The maximum target extent is 15m and it is initially nose-on to the radar.

In the case of a complex target, 22 scatterers are used to represent the various scattering points on the aircraft. These points realistically represent the dominant scatterers from an aircraft. The maximum target extent is 10m. The dimensions are as given in Figure 5.2. The leading edge scatterers, ie, those facing the radar, will be assigned higher signal returns. Note that, in both cases, the target is assumed to be in the same horizontal plane as the radar so that all its z-coordinates are zero. The rotational

speed of the target, ω , is assumed to be 0.002 rad/s, which may not typically represent the yaw dynamics of a rotating target. This value of ω is chosen in order to match the radar parameters selected to avoid image distortion. The key point of the ISAR technique is that crossrange information can be extracted as long as there is rotational motion of the target. In a real world, a target's motion will have a rotating component in which the radar can process to track and therefore image the target's RCS in the crossrange direction.

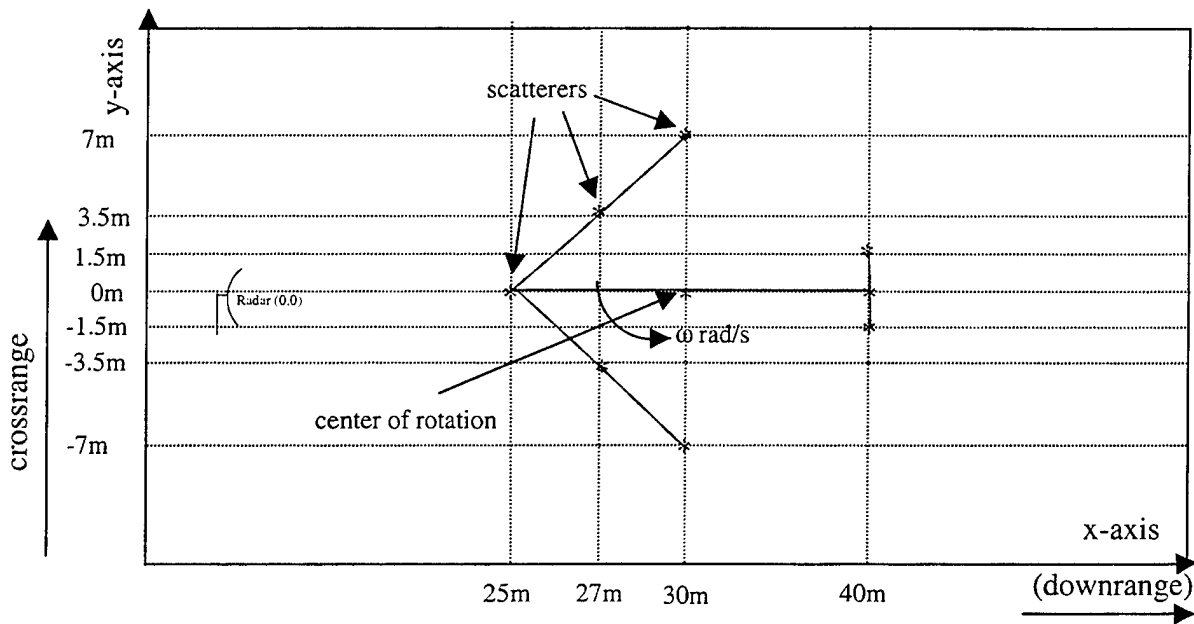


Figure 5.1 Model of a Simplified Aircraft with 9 Scatterers.

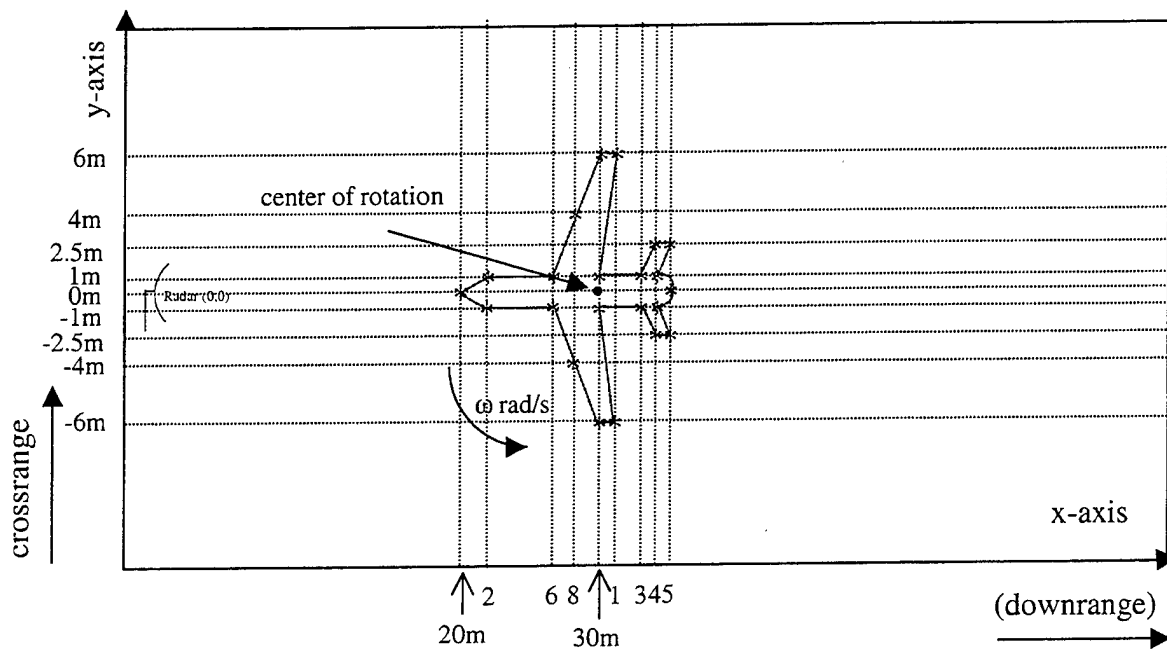


Figure 5.2 Model of a Complex Aircraft with 22 Scatterers.

C. RADAR AND TARGET PARAMETERS

The following radar and target parameters were selected:

1. Carrier frequency, f_0 = 40 GHz
2. PRF, f_p = 10 kHz
3. Stepped frequency step size, Δf = 1 MHz
4. No. of stepped frequency steps, N = 512
5. No. of burst for ISAR processing, M = 100
6. Pulse width, τ = 0.1 μ s
7. Maximum target extent, E = 15m
(radar designed to image small fighter aircraft only)
8. Target rotational frequency, ω = 0.002 rad/s
9. Unambiguous downrange window, R_u (W_d) = 150 m

D. STEPPED FREQUENCY PROCESSING PARAMETERS AND REQUIREMENTS

The following parameters were computed and verified to meet the stepped frequency requirements as delineated in Chapter II.

1. Receiver instantaneous bandwidth, B_{inst} ($= 1/\tau$) = 10 MHz
2. Frequency step size, $\Delta f \leq 1/\tau$? ($10^6 \leq 10^7$?) = YES
3. Frequency step size, $\Delta f \leq c/(2E)$? ($10^6 \leq 10^7$?) = YES
4. Effective signal bandwidth, B_{eff} ($= N\Delta f$) = 512 MHz
5. Conventional downrange resolution, $\Delta r_{conventional}$ = 15 m

6. Stepped frequency downrange resolution, Δr = 0.293 m
7. Conventional unambiguous downrange window, $R_{u,conventional} = 15\text{km}$
8. Stepped frequency unambiguous downrange window, $R_u (=W_d) = 150\text{ m}$
9. $R_u > E$? (150m > 15m?) = YES
10. Pulsewidth, $\tau \geq \frac{2E}{c}$? ($10^{-7} \geq 10^{-7}$?) = YES

E. ISAR PROCESSING PARAMETERS AND REQUIREMENTS

From the radar parameters, the ISAR requirements were verified to meet the Nyquist sampling requirement to prevent aliasing.

1. Integration time, T_i = 5.12 s
2. doppler resolution, Δf_d = 0.195 Hz
3. Crossrange resolution, Δr_c = 0.366 m
4. Unambiguous crossrange window size, W_c = 36.6 m
(max target width processed)
5. Angle rotated by target during integration time, ψ = 0.01 rad
6. Maximum allowed rotation angle, ψ_{max} = 0.011 rad
7. $\psi < \psi_{max}$? (0.010 rad < 0.011 rad?) = YES
8. Effective PRF, $f_{p,effective}$ = 19.5 Hz
9. Twice doppler frequency, $2f_{d(max)}$ = 17 Hz
10. $f_{p,effective} > 2f_{d(max)}$? (19.5 Hz > 17 Hz?) = YES

VI. SIMULATION RESULTS & DISCUSSION

The primary objective of the simulation is to image an aircraft target comprised of multiple scatterers. As the downrange resolution of the radar processing is dependent on the effective bandwidth, it is important to visualize how the effective bandwidth of a stepped frequency waveform is obtained, and the undesirable effects of target rotation on the image quality. The first two parts of this section will focus on performing simulations to illustrate these two concepts. It will be followed by simulating the stepped frequency and ISAR processing techniques to image both simple and complex targets.

A. BANDWIDTH OF TRANSMITTED WAVEFORM

From Chapter II, it can be seen that the high downrange resolution is obtained from an wide effective bandwidth, B_{eff} . Figures 6.1 through 6.3 show the simulation results for the following parameters. The figures demonstrate that the effective bandwidth is $N\Delta f$.

- | | | |
|----|-----------------------------------|---------------|
| a. | Carrier frequency, f_c | = 1 GHz |
| b. | Number of datapoints for FFT | = 512 |
| c. | Stepped frequency, Δf | = 5MHz |
| d. | Number of pulses, N | = 12 |
| e. | $N\Delta f$ | = 60MHz |
| f. | Pulsewidth, τ | = 0.1 μ s |
| g. | Pulse repetitive frequency, f_p | = 10kHz |

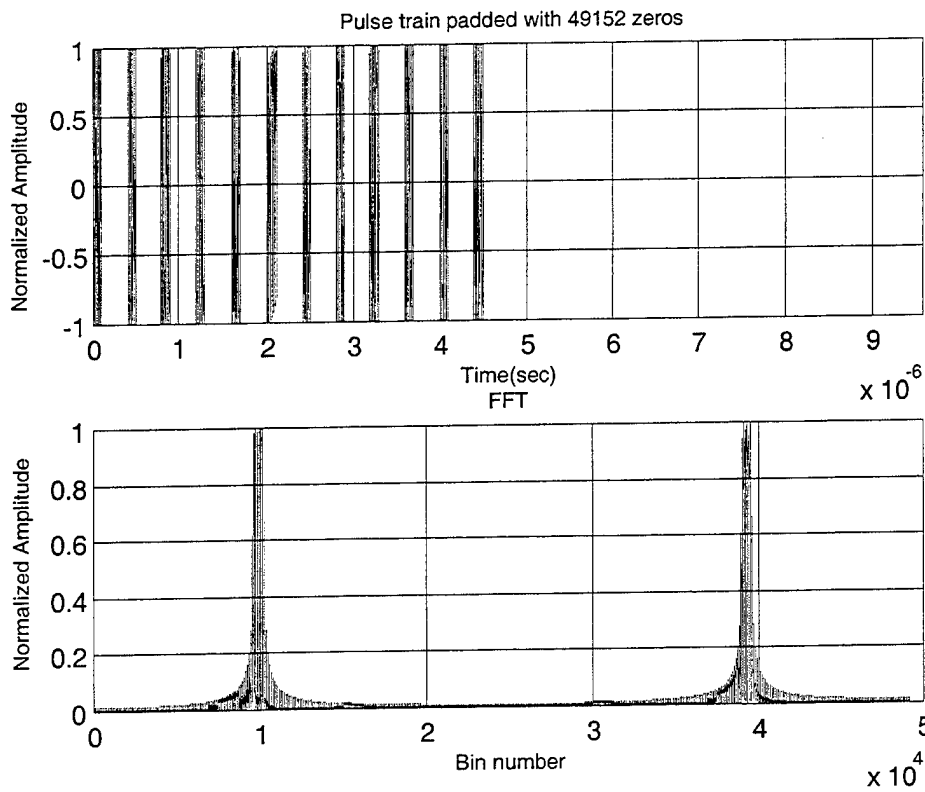


Figure 6.1 Transmitted Pulse Spectrum after FFT.

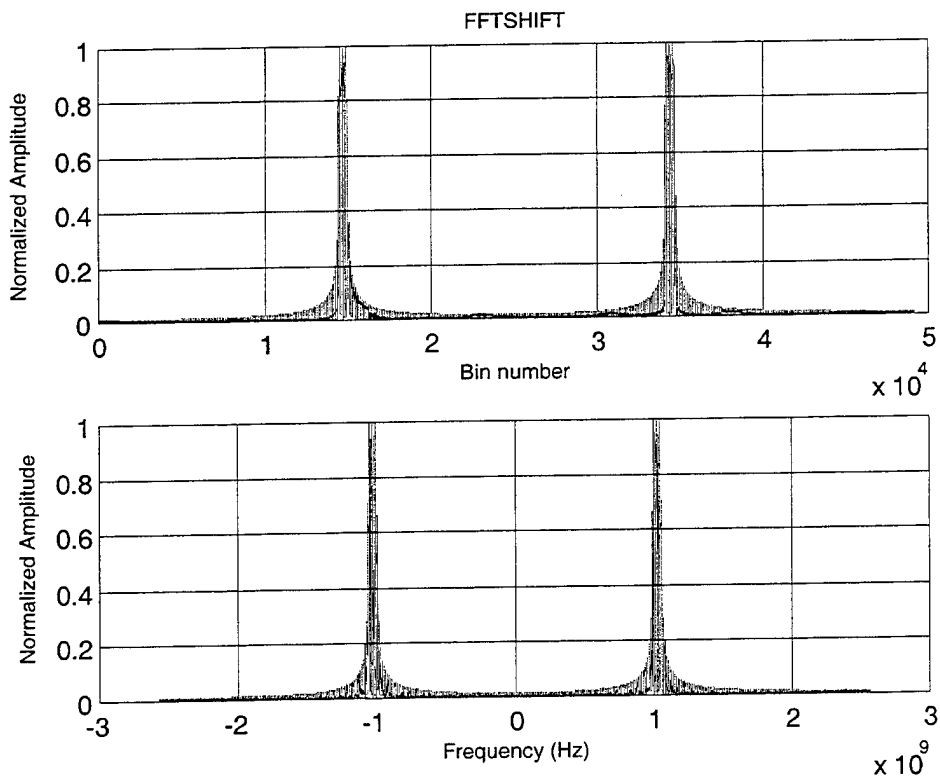


Figure 6.2 Transmitted Pulse Spectrum after FFTSHIFT.

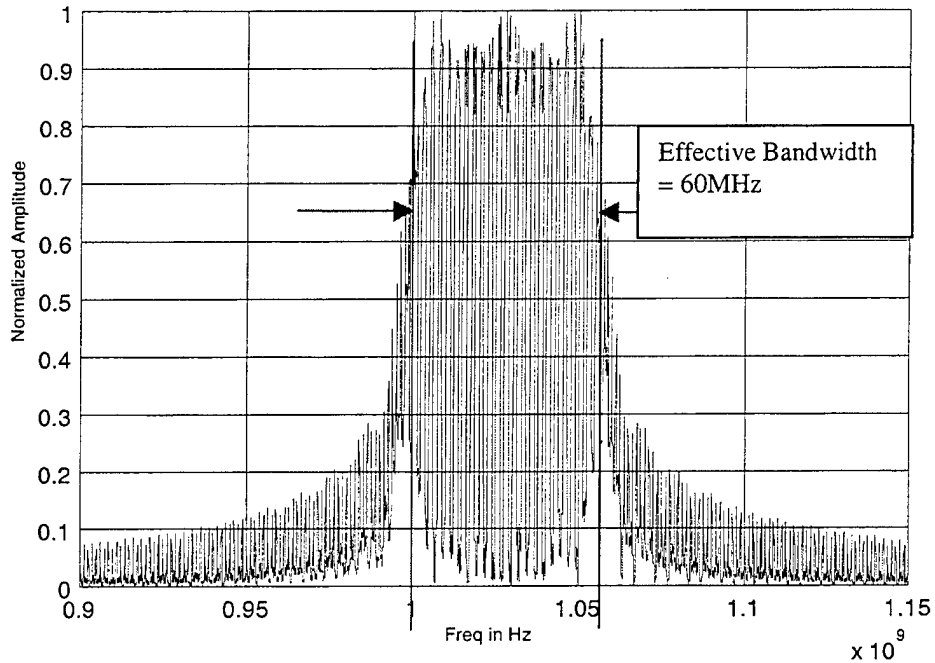


Figure 6.3 Expanded Pulse Spectrum after FFT and FFTSHIFT (Positive Frequency).

In the simulation, 12 stepped frequency pulses are transmitted and the signal returns are processed using FFT. A characteristic of the function FFT is that the positive frequencies lie on the left side of the spectrum. FFTSHIFT is used to properly order the spectrum. The transmitted pulses, FFT and FFTSHIFT processed spectrums are shown in Figure 6.1 and Figure 6.2. Figure 6.1 shows both the transmitted waveform and its spectrum, while Figure 6.2 shows the FFTSHIFT spectra with the x-axis scaled as FFT bin number and frequency, respectively. By keeping only the positive frequency spectrum through filtering, the step frequency spectrum showing an increased bandwidth can be extracted. The simulation shown in Figure 6.3 demonstrates that the stepped frequency waveform exhibits an effective bandwidth of 60MHz, which is obtained from the product of the frequency step size, Δf , and the number of pulses transmitted, N .

B. TRACKING WINDOW AND EFFECTS OF TARGET ANGULAR VELOCITY

Chapter IV discussed the effects of the target angular velocity on both the range and doppler profiles, namely, range-doppler interaction and cell migration. The image effects include shifting of range cells as well as blurring.

With the radar and target parameters chosen for the design, we can map the tracking window in which unambiguous downrange and crossrange information can be derived. The tracking window dimensions are determined by the unambiguous downrange (W_d) and the crossrange window (W_c), respectively. Any scatterer that falls outside this window will wrap around and be incorrectly displayed in the tracking window. The dimensions of the tracking window are shown in Figure 6.4.

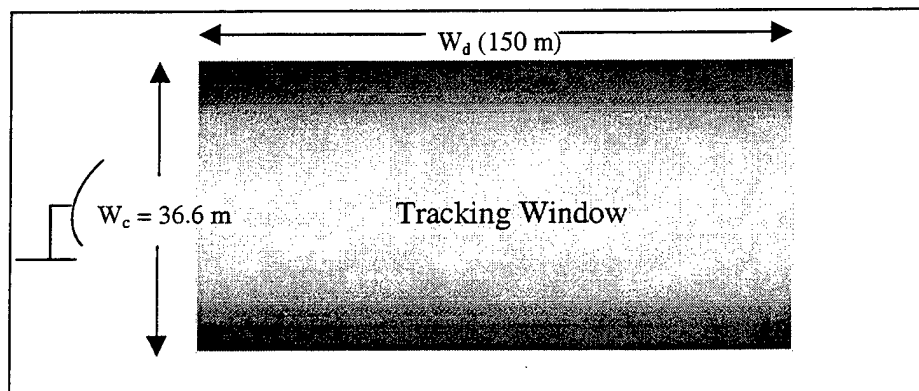


Figure 6.4 Tracking Window.

The effect of range wraparound can be shown from the following case, whereby the tracking window stretches from 4500 m to 4650 m ($R_u = 150\text{m}$). A scatterer located at 4690 m will appear at 40 m in the tracking window. This is illustrated in Figure 6.5.

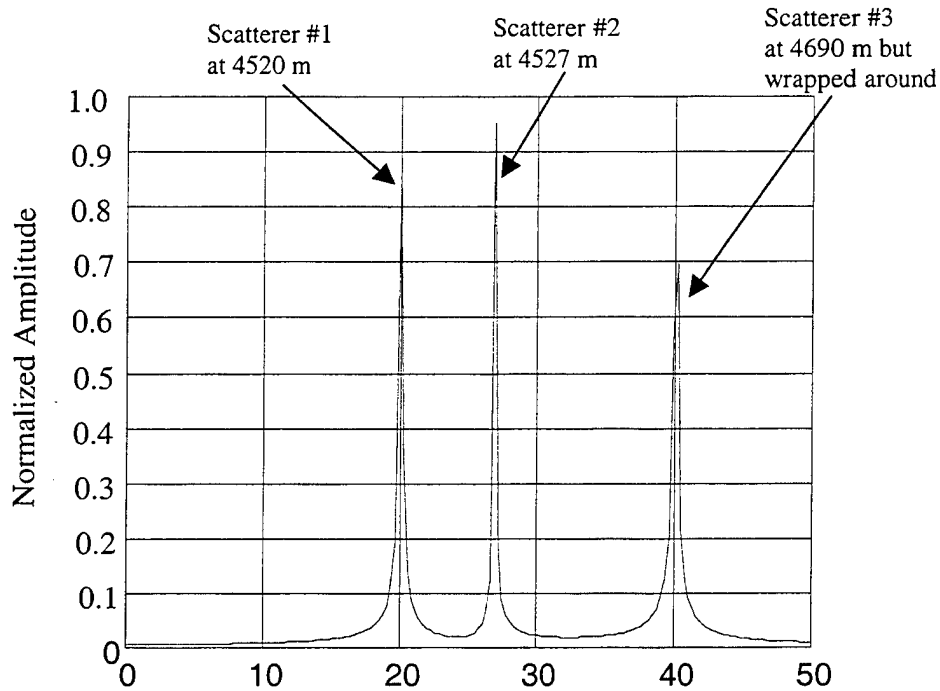


Figure 6.5 HRR (downrange) Profile – Range Wraparound.

If the target rotation does not meet the requirements put forth in Chapter IV, the result will be a degradation of the range and doppler (or crossrange) profiles, depending on the location of the scatterers from the center of rotation and the radar-target line-of-sight. In the simulation, scatterers were defined at different locations from the center of rotation. One of the scatterers is always in the center of the rotation for comparison purposes. Two different scenarios are tabulated in Table 1. Note that the threshold for the downrange and crossrange radial distances from the center of rotation are computed from Equation 4.7 to be approximately 14 m and 18 m respectively. This means that, for this design, the crossrange window width (about 18m in radius) is the limiting factor instead of the threshold distance from the center of rotation to avoid spreading and range walking effects of the range profile. A scatterer located at the same range to the radar as

the scatterer located at the center of rotation, but at different crossrange will result in a shifting of the range profile in the downrange direction. This will be illustrated in the output graphs for scenario one. A similar explanation holds for scatterers having a different downrange but with the same crossrange. The observation is illustrated in the output graphs from scenario two.

	Coordinates (x,y) of Scatterer 1 (center of rotation)	Coordinates (x,y) of Scatterer 2	Coordinates (x,y) of Scatterer 3	Coordinates (x,y) of Scatterer 4
Scenario One	(4530,0)	(4540,0)	(4560,0)	(4600,0)
N_d	-	< 0.5	< 0.5	< 0.5
N_c	-	< 0.5	> 0.5	> 0.5
Scenario Two	(4520,7)	(4530,5)	(4530,17)	
N_d	-	<0.5	\cong 0.5	
N_c	-	<0.5	<0.5	

Table 1 Effects of Target Rotation – Two Scenarios.

1. Scenario One

In this scenario, the four scatterers are located in a straight line along the radar-to-target center line, as shown in Figure 6.6a. Figure 6.6b shows the downrange profile, which does not indicate any excessive ($N_{c,d}$) spreading effects, as expected. However, in the crossrange profile, scatterers 3 (downrange separation of 30m) and 4 (downrange separation of 70m) do experience undesirable spreading and range walking effects. The spreading and range walking effects are shown in Figures 6.6c and 6.6d respectively. This is because both scatterers exceeded the threshold radial distances. From these

limitations, the downrange tracking window has been optimized to work in the range of about $\pm 18\text{m}$ from the target's center of rotation to provide an undistorted downrange profile.

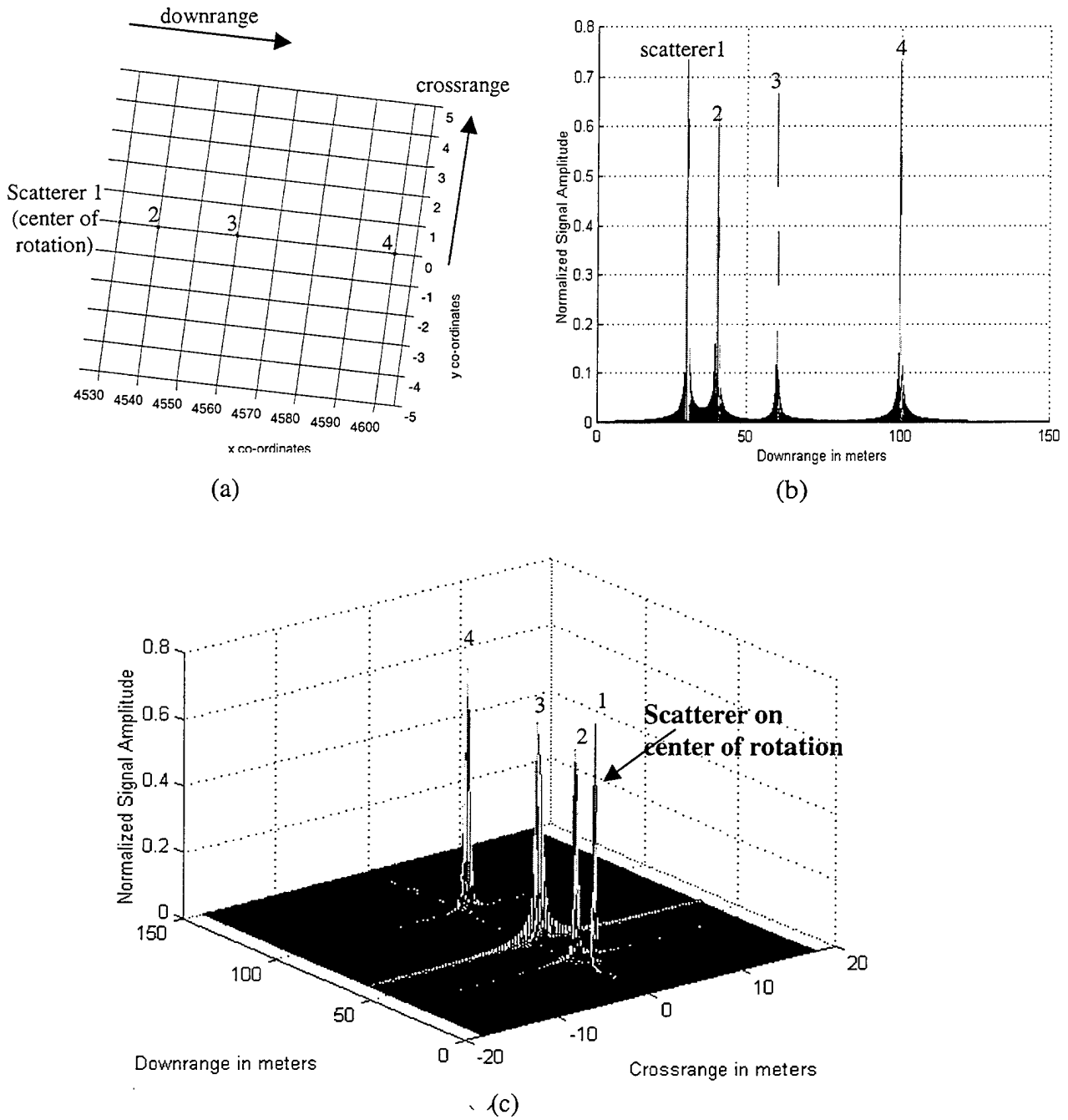


Figure 6.6 (a) Location of Scatterers, (b) Downrange Profile (c) 3-D View Depicting Target Spreading and Range Walking Effects.

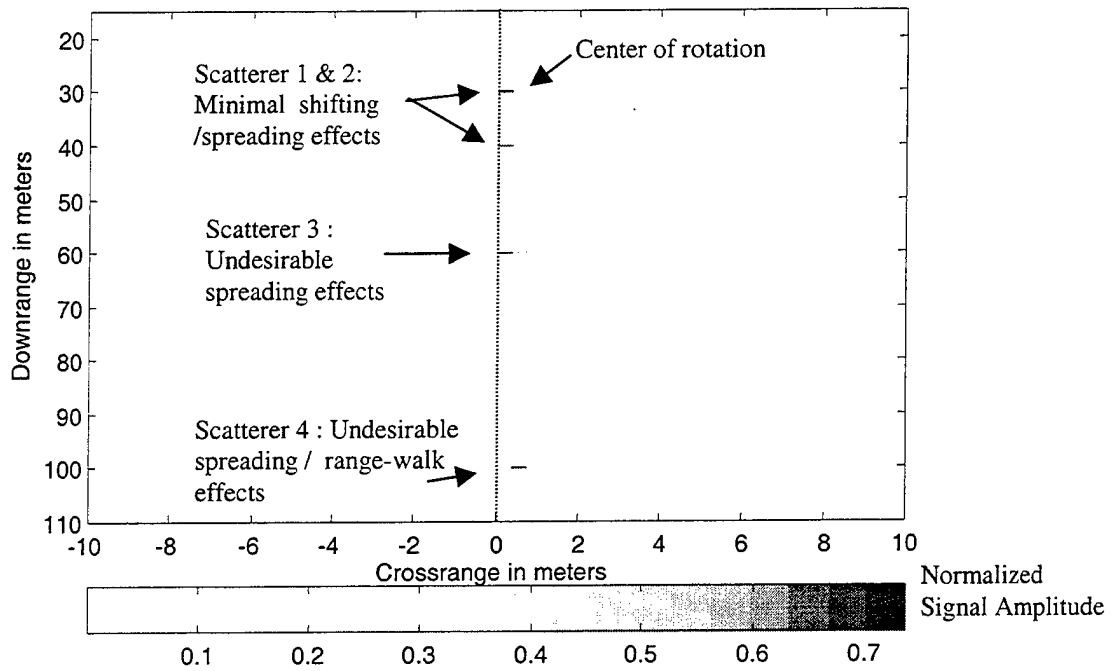
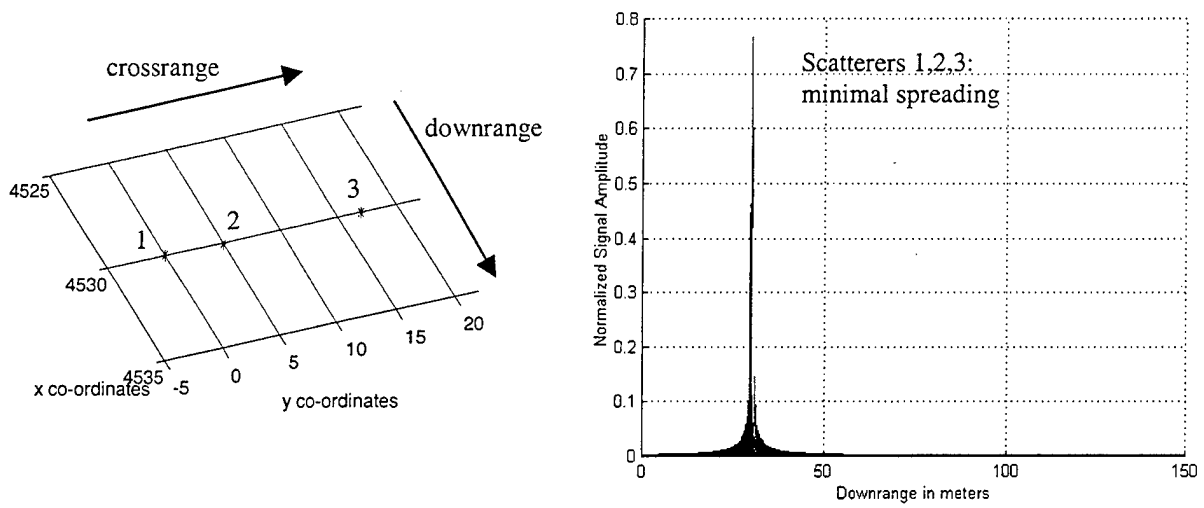


Figure 6.6 (continued) (d) Plan View Depicting Target Spreading and Range Walking Effects.

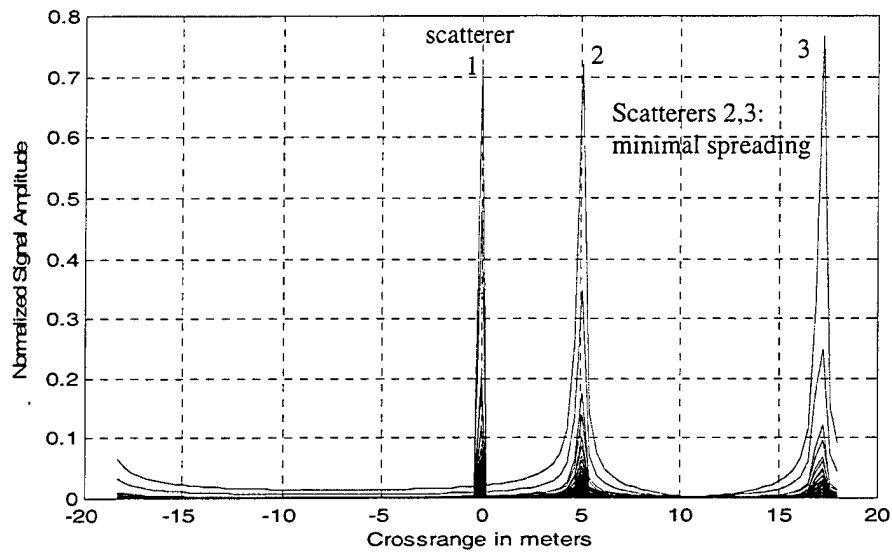
2. Scenario Two

For this scenario, the crossrange tracking window of approximately $\pm 18\text{m}$ has been noted in earlier paragraphs as the limiting width for an undistorted downrange profile. The Matlab plots given in Figures 6.7a through d verify this.



(a)

(b)



(c)

Figure 6.7 (a) Location of Scatterers, (b) Downrange Profile, (c) Crossrange Profile.

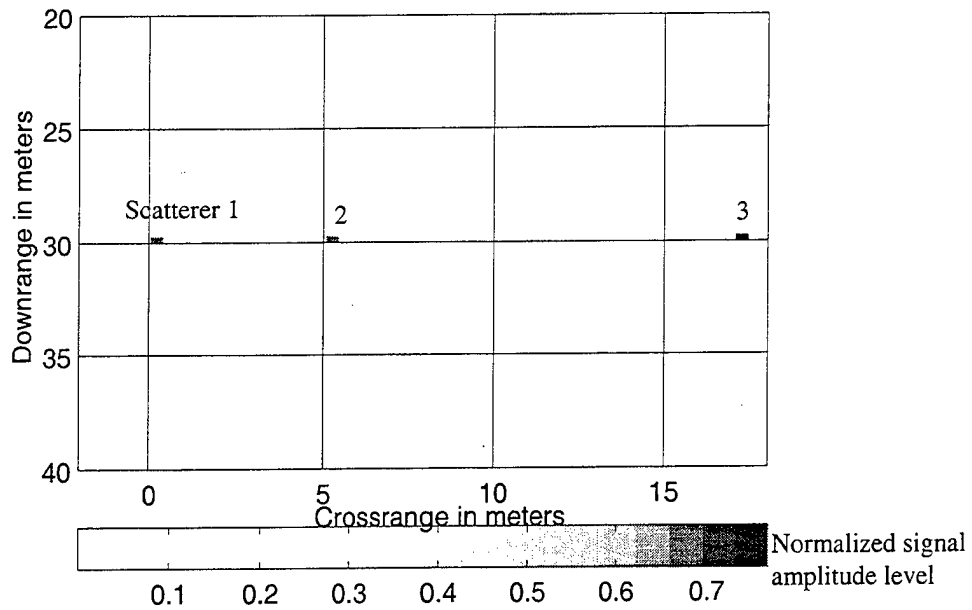


Figure 6.7 (continued) (d) Plan View Depicting Minimal Target Spreading and Range Walking Effects.

In summary, the size of the optimized tracking window depends largely on the rotational speed, the integration time and the distance of the scatterer from the center of rotation. In the design, the optimized tracking window, whereby the target image remains undistorted in both downrange and crossrange dimensions due to its rotation, is given in Figure 6.8.

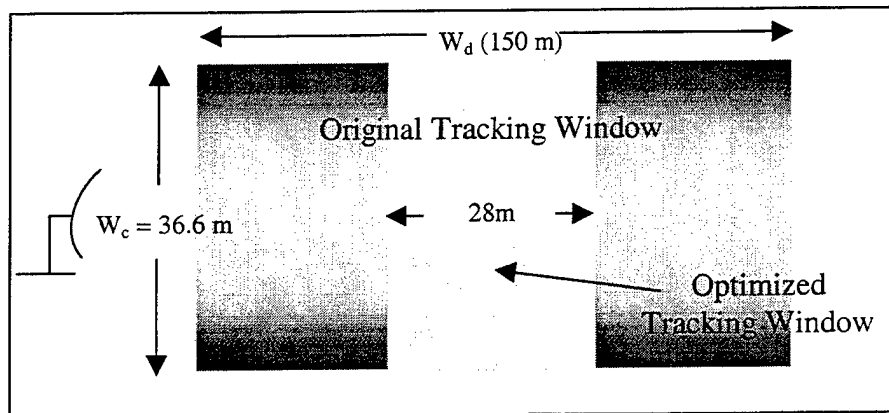


Figure 6.8 Optimized Tracking Window.

C. IMAGE OF SIMPLE TARGET

The image of the simple target in Figure 5.1 is shown in Figures 6.9 and 6.10. The RCS returns from the 9 scatterers are clearly shown in the mesh plot of Figure 6.9. All scatterers were defined within the optimized tracking window to avoid degradation of the downrange and crossrange profiles. As seen in Figure 6.9, the amplitudes of the scatterers' image vary depending on the amount of doppler change as seen by the tracking radar during the processing integration time. Two scatterers located on opposite sides of the center of rotation will experience different doppler changes during the integration time, and consequently the amount of spreading, and hence their image amplitudes will be different. The undistorted quality of the image is shown in Figure 6.10.

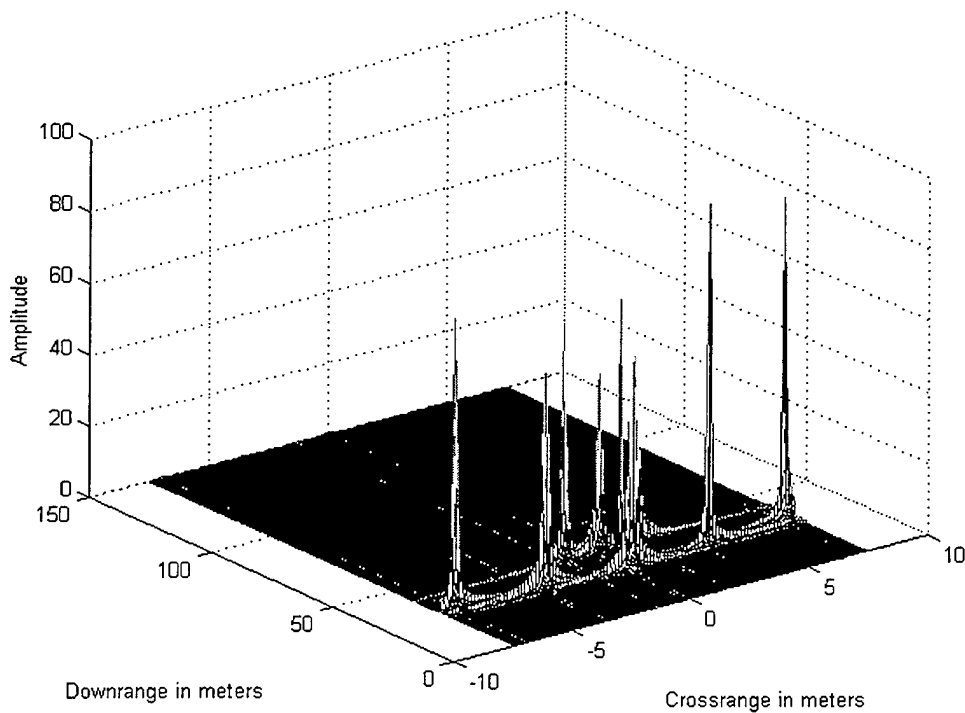


Figure 6.9 RCS Returns (Mesh Plot) from 9 Scatterers on a Simple Target.

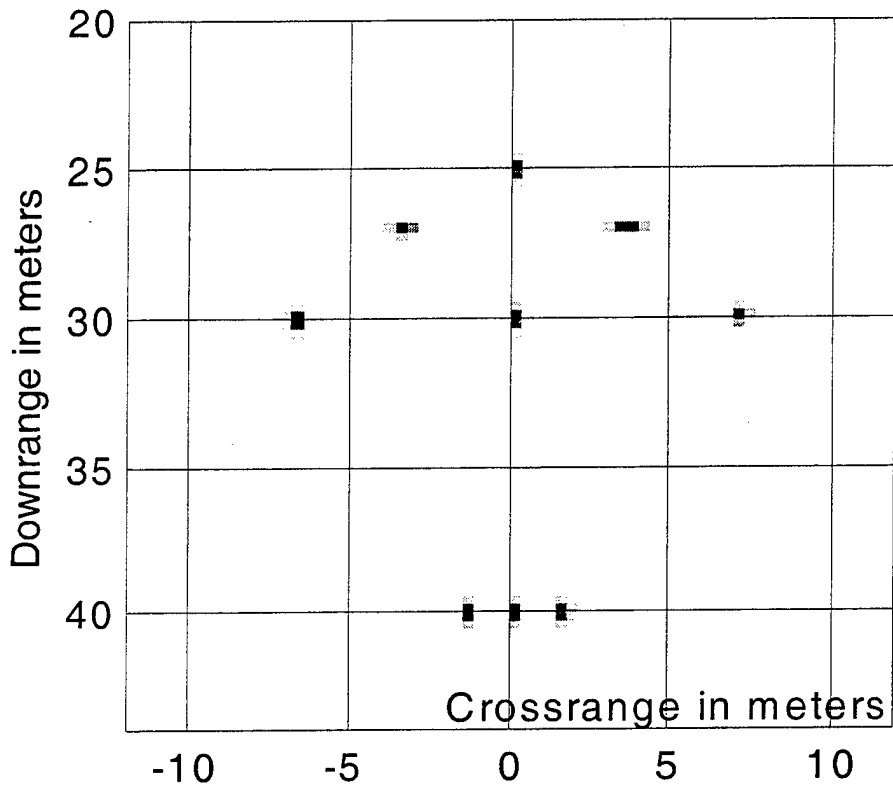


Figure 6.10 Undistorted RCS Returns (Plan View) from 9 Scatterers on a Simple Target. Illustrated in Figure 5.1.

D. IMAGE OF COMPLEX TARGET

The image of the complex target in Figure 5.2, which simulates an aircraft, is plotted in Figure 6.11. The asymmetry of the image due to the different shifting and spreading of scatterers is evident.

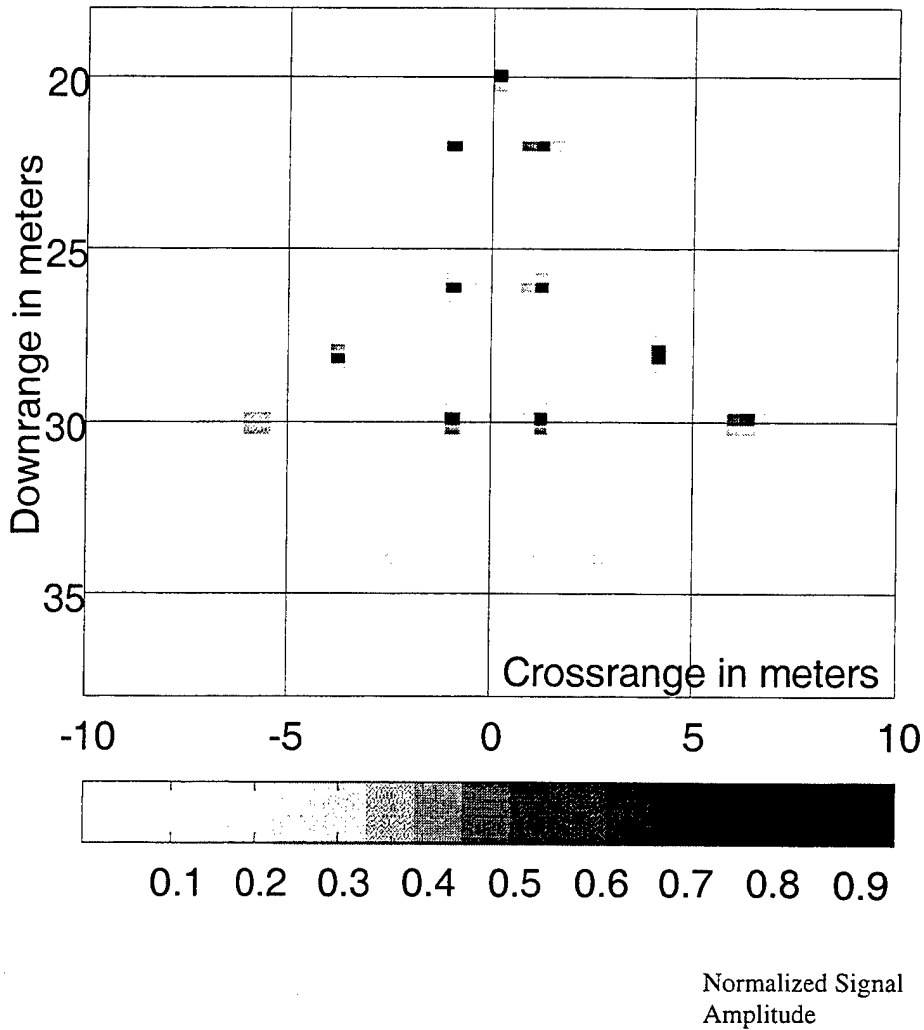


Figure 6.11 RCS Returns (Plan View) from 22 Scatterers on the Complex Target (RCS of leading edge scatterers higher than those on trailing edge). Illustrated in Figure 5.2.

THIS PAGE INTENTIONALLY LEFT BLANK

VII. CONCLUSIONS AND RECOMMENDATIONS

A. CONCLUSIONS

This thesis employed both stepped frequency and ISAR processing techniques to generate an image from the returns of targets, both simple and complex. The parameters that affect the downrange and crossrange tracking windows, range resolution and ambiguities were examined. Simple targets with few scatterers were used to identify the effects of radar parameters on image quality. This resulted in the formulation of guidelines for an optimized window in the design of the imaging simulation program. Finally, a detailed point scatterer model of a complex aircraft was run through the simulation and the image plotted. Scatterers close to one another could easily be discerned in the image.

The stepped frequency and ISAR processing techniques are useful in obtaining high resolution images of targets in both downrange and crossrange. Resolutions of less than one meter are possible using these two complementary techniques. Together with velocity compensation techniques discussed in earlier thesis studies [3], imaging of targets comprised of multiple RCS scatterers are possible. Nevertheless, it is important to choose the correct radar parameters in order to avoid aliasing and range spreading and walking effects due to the target's rotational motion.

B. RECOMMENDATIONS

Further investigations can be made in the imaging techniques. As the ISAR processing is a conventional processing technique, it assumes that the doppler shifts are

constant during the integration period. If the scatterers drift out of their range cells or their doppler frequency shifts become time varying, the image will become blurred. Efficient motion compensation techniques need to be employed for each scatterer, as opposed to conventional motion compensation which applies compensation to the target as a whole. A recommended approach is to use the Joint Time Frequency Analysis [6]. This method replaces the conventional radar Fourier transform with a high-resolution time-frequency transform, and maps 2-D range-Doppler image frame into a 3-D time-range-Doppler image cube. By sampling in time, a time sequence of 2-D range-Doppler images with superior resolution can be obtained.

APPENDIX A: STEPPED FREQUENCY WAVEFORM PROGRAM CODE

```

%%%%
% Program Code for Generation of Effective Bandwidth of Step %
% Frequency Waveform %
%%

clear all

%Initialize
format long
pw = 0.1e-6;           %pulsewidth
fc=1.0e9;             %carrier frequency
Tp = 4*pw;           %PRT
fs = 1/Tp;           %sampling frequency
pul=12;              %number of pulses per train/burst
del_f=zeros(1,pul); %initialise stepped frequcies
                    %stepped frequency step size

for nn=1:pul
    del_f(nn)=5e6*(nn-1);
end

%Compute f(t) with 64 sample points per pulse
datapoint=512;       %number of data points
del_t=pw/datapoint; %smallest time resolution
f=zeros(1,pul*(Tp/pw)*datapoint); %Initialisse f(n)
for pulse=1:pul;
    temp1=(pulse-1)*Tp/pw*datapoint; %define the start of each of pulses
    % (temp1=64x4=256 pts,ie, 0,256,512,...,32512 or 64x4x127))
    for nn=(temp1):((datapoint)+temp1)
        n=floor(nn); % integer value
        t=n*del_t + (del_t/2); % take time of each sub-pulse to be the mid-point bet 2 sub-pulses
        f(n+1)=cos(2*pi*(fc+del_f(pulse))*t); % define the amplitude of the pulses
    end
end

%Zero padding after last pulse for better frequency resolution
padzero=2*pul*(Tp/pw)*datapoint; %add 128 NULL pulses after the last pulse
last=pul*(Tp/pw)*datapoint; %last point on pulse train
int=floor(last); %integer value
f((int+1):padzero)=zeros(1,padzero-int); %pad with zeros
A=[0:padzero-1];
t(1:padzero)= del_t*A; % set time scale

%Plot the pulse train
figure(1);
subplot(2,1,1)
tlimit = pw/datapoint*(padzero-1);
plot(t,f,'xlabel(\fontsize{8}Time(sec)'),
      ylabel(\fontsize{8}Amplitude')
      title([\fontsize{8}Pulse train padded with ',num2str(padzero)', ' zeros'])
      axis([0 tlimit -1 1]);
grid on

```

```

%Compute spectrum of pulse train
subplot(2,1,2)
FT=(fft(f));
temp=length(abs(FT));
plot(abs(FT),xlabel('\fontsize{8}Bin number'),ylabel('\fontsize{8}Amplitude')
title('\fontsize{8}FFT')
grid on

%Plot spectrum using FFTSHIFT
figure(2)
subplot(2,1,1)
FFTSHT=fftshift(FT);
plot(abs(FFTSHT),xlabel('\fontsize{8}Bin number'),ylabel('\fontsize{8}Amplitude')
title('\fontsize{8}FFTSHIFT')
grid on

%Plot spectrum in frequency domain
subplot(2,1,2)
deltafreq = 1/(pw/datapoint*padzero);      % frequency stepsize
f = ((1:padzero)-(padzero/2))*deltafreq;
plot(f,abs(FFTSHT));
xlabel('\fontsize{8}Frequency (Hz)'),ylabel('\fontsize{8}Amplitude')
grid on
Fmax=max(abs(FFTSHT));

figure(3)
deltafreq = 1/(pw/datapoint*padzero);
f = ((1:padzero)-(padzero/2))*deltafreq;
ff=abs(f);
plot(f,abs(FFTSHT)/Fmax);
xlabel('\fontsize{8}Freq in Hz'),ylabel('\fontsize{8}Amplitude')
grid on
figure(3), axis([0.9e9 1.15e9 0 1])

%%

```


APPENDIX B : STEPPED FREQUENCY AND ISAR PROCESSING PROGRAM

CODES

```
%% Program Code for Stepped Frequency and ISAR Simulation in Imaging Radar %%
%% Multiple scatterers rotating about a reference point

%Process a pulse train for doppler and range information
clear all
format long

%%INITIALIZATION%%

%Radar parameters
N=512;           % number of pulses in one burst
fp=10e3;        % PRF
Tp=1/fp;        % interpulse period
T=N*Tp;         % total observation time
df=1/T;         % frequency increment
fc=40e9;        % carrier frequency
c=3e8;          % speed of light
wave=c/fc;      % wavelength
step=1e6;       % stepped frequency step size
taucm=1/(N*step); % compressed pulse width
dr=c*taucm/2;   % compressed down-range resolution
fpeff=fp/N;     % effective PRF using stepped frequency (used in cross range)

%Define stepped frequency
for nn=1:N
    del_f(nn)=step*(nn-1);
end

%%Target generation%%

%Define Radar position
radarpos=[0 0 0]; %define radar position

%Define initial scatterers' positions on target
x=[4530 4525 4527 4527 4530 4530 4540 4540];
y=[0 0 -3.5 3.5 -7 7 0 -1.5 1.5];
z=[0 0 0 0 0 0 0 0 0];

center=[4530 0 0]; %center of rotation
r = sqrt((x-radarpos(1)).^2+(y-radarpos(2)).^2+(z-radarpos(3)).^2);
%Radial distance of scatterers from radar

%Compute no. of down-range bins
```

```

Ru=c/(2*step);           %unambiguous down-range window = 150m (0.29mx512)
Rumax=c/(2*fp);         %unambiguous maximum detection range (15000m)
numdrbin= Rumax/Ru;     %no. of down-range bins**(15000/150=100)

%Compute number of pulse burst
temp=mod(r,Ru)/Ru;
mbin=temp*N;
rngno = floor(r./Ru);   % range gate no.
ntarg=length(mbin);    % no of scatterers
M=floor(Rumax/Ru);

%Assign velocity to each scatterer
w=0.002;                % rotation speed of target in rad/s in x-y plane***
                        %positive = clockwise

%Determine doppler velocity for each scatterer at each time frame, ie, every N pulses for M bursts.
ANS= angle2(w,center,x,y,z,radarpos,ntarg,M,N,Tp,wave); %doppler velocity
fd=ANS(:,1:M);
vr=ANS(:,M+1:2*M);
range_time=ANS(:,2*M+1:3*M); %range of scatterer at different time throughout Ti

disp(['No. of scatterers defined : ',num2str(ntarg)]);
disp(['Max. unambiguous detection range : ',num2str(Rumax)]);
disp(['Unambiguous range window : ',num2str(Ru)]);
disp(['The calculated coarse downrange bin # : ',num2str(rngno)]);
disp(['Calculated fine downrange bin # : ',num2str(mbin)]);

%Generate Is and Qs
I=zeros(N,M);
Q=zeros(N,M);
dt=2*dr/c;              %time separation between samples

A=ones(1,ntarg);
B=5*ones(1,11);
A(1:11)=B;              %define dominant scatterers on leading edge of aircraft

for tgt=1:ntarg
    for time=1:M*N ;
        tm(tgt,time)=(2/3e8)*(range_time(tgt,ceil(time/N)) ); %2Rn/c
    end

    for m=1:M
        for n=1:N
            I(n,m,tgt)=A(tgt)*cos(2*pi*(fc+del_f(n)+fd(tgt,m)).*tm(tgt,((m-1)*N+n)));
            Q(n,m,tgt)=A(tgt)*sin(2*pi*(fc+del_f(n)+fd(tgt,m)).*tm(tgt,((m-1)*N+n)));
        end
    end
end

II=zeros(N,M);
QQ=zeros(N,M);
for tg=1:ntarg
    II=II+I(:,:,tg);
    QQ=QQ+Q(:,:,tg);
end

```

```

%Add noise if required
No=randn(N,M)*0.05*0;
I=II+No; Q=QQ+No;
%save c:\files\echoes I Q -ASCII

%Plot the position of scatterers wrt radar
figure(1)          %3-D plot
subplot(2,1,1)
plot3(x, y, z, '*')
xlabel('x co-ordinates')
ylabel('y co-ordinates')
zlabel('z co-ordinates')
grid on; view(3);

figure(1), hold on    %Plan view
subplot(2,1,2)
plot3(x, y, z, '*')
xlabel('x co-ordinates')
ylabel('y co-ordinates')
zlabel('z co-ordinates')
grid on; view(45,90);
axis([min(x)-5, max(x)+5, min(y)-5, max(y)+5, -1, 1])

%%%%
%PROCESSING OF TARGET RETURNS%
%%

%Processing Target Returns using IFFT to obtainb HRR profile
it=0;          %initialise no. of scatterers detected
bincourse=0; binfine=0; dopbin=0; %initialise range and doppler bin of detected scatterer

Z1=zeros(M,N);

%FFT of the time samples will give the HRR profile
for m=1:M      %M range bins
    A1=I(:,m)-j*Q(:,m);
    B1=fft(A1); As1=ifft(A1);
    Z1(m,:)=As1(:).';
end

figure(2) %plot HRR
rngfaxis=([0:N-1]*dr);
for t=1:M
    plot(rngfaxis,abs(Z1(t,:))) %/N
    hold on
end
xlabel('Downrange in meters')
ylabel('Amplitude')
grid on

%Processing Target Returns using FFT to obtain crossrange profile

Z2=zeros(N,M);
for p=1:N

```

```

    B2=fft(Z1(:,p)); B3=fftshift(B2);
    Z2(p,:)=B3(:).';
end

figure(3) %plot doppler profile
dfstep=fp/(N*M);
drc=(3e8*dfstep)/(2*w*fc);
craxis=([0:M-1]-M/2)*drc;
for n=1:N
    plot(craxis,abs(Z2(n,:))/M)
    hold on
end
xlabel('Crossrange in meters')
ylabel('Amplitude')

grid on

figure(4)
x=linspace(-((M-1)-M/2)*drc ,((M-1)-M/2)*drc, M);
y=linspace(0, (N-1)*dr, N);
mesh(x,y,abs(Z2))
xlabel('Crossrange in meters')
ylabel('Downrange in meters')
zlabel('Amplitude')

figure(5)
x=linspace(-((M-1)-M/2)*drc ,((M-1)-M/2)*drc, M);
y=linspace(0, (N-1)*dr, N);
mesh(x,y,abs(Z2))
xlim=((M-1)-M/2)*dfstep;
ylim=(N-1)*dr;
zlimit=0;
for f=1:M
    zlimit(f)=max(abs(Z2(:,f)));
end
zzlimit=max(zlimit);
n=21;
mymap=[ 1.0 1.0 1.0;
        1.0 1.0 0.9;
        1.0 1.0 0.8;
        1.0 1.0 0.7;
        1.0 1.0 0.6;
        1.0 1.0 0.5;
        1.0 1.0 0.4;
        1.0 1.0 0.3;
        1.0 1.0 0.2;
        1.0 1.0 0.1;
        1.0 1.0 0.0;
        1.0 0.9 0.0;
        1.0 0.8 0.0;
        1.0 0.7 0.0;
        1.0 0.6 0.0;
        1.0 0.5 0.0;
        1.0 0.4 0.0;
        1.0 0.3 0.0;

```

```

1.0 0.2 0.0;
1.0 0.1 0.0;
1.0 0.0 0.0;];

colormap(mymap)

imagesc(x,y,abs(Z2));
colorbar('hori')
figure(5)
xlabel('Crossrange in meters')
ylabel('Downrange in meters')
zlabel('Amplitude')
view(0,90)

%%%%%%%%%%%%%%%%%%%%%%%%%%%%%%%%%%%%%%%%%%%%%%%%%%%%%%%%%%%%%%%%%%%%%%%%

%%%%%%%%%%%%%%%%%%%%%%%%%%%%%%%%%%%%%%%%%%%%%%%%%%%%%%%%%%%%%%%%%%%%%%%%
%Function to Compute Radial Velocity of Individual Scatterers %
%%%%%%%%%%%%%%%%%%%%%%%%%%%%%%%%%%%%%%%%%%%%%%%%%%%%%%%%%%%%%%%%%%%%%%%%

function ANS=angle2(w,center,x,y,z,radarpos,ntarg,M,N,Tp,wave)
format long
radius=sqrt((center(2)-y).^2+(center(1)-x).^2); %radius of scatterer from center of rotating circle, vector
range = sqrt((x-radarpos(1)).^2+(y-radarpos(2)).^2+(z-radarpos(3)).^2)%center-radar distance, vector
range_ref=sqrt((center(1)-radarpos(1)).^2+(center(2)-radarpos(2)).^2+(center(3)-radarpos(3)).^2);

v=w*radius;

%Determine sign of radial velocity from gradient formula
delta_x=x-radarpos(1);
delta_y=y-radarpos(2);
grad_ref=(center(2)-radarpos(2))/(center(1)-radarpos(1)); %gradient of center-radar vector
grad=(delta_y)/(delta_x);

%Determine x and
c=range;
b=radius;
a=range_ref;

% Vector OR : radar-center vector
OR=[center(1)-radarpos(1); center(2)-radarpos(2)];

% Vector RA : center to scatterer
for tg=1:ntarg
RAx(tg)=[x(tg)- center(1)];
RAy(tg)=[y(tg)- center(2)];
end
RA=[RAx;RAy];

%Compute length of OR and RA
ORMag=range_ref;
RAMag=radius;

```

```

%Compute angle between OR and RA ie radar-center and center-scatterer
%Quadrant 1

for tg=1:ntarg
    if RAmag(tg)~=0
        theta1(tg)=acos( dot(OR,RA(:,tg)) /(ORmag*RAmag(tg)) ); %dot product between vectors OR & RA
        %verified
    else
        theta1(tg)=pi;
    end
end

%Compute theta for M pulses & x and y co-ordinates of scatterers over time
for tg=1:ntarg
    %check which quadrant scatterer is in
    if ( ( grad(tg)>grad_ref ) | (( grad(tg)==grad_ref ) & (range(tg)>range_ref)) ) %quadrant 1

        for m=1:M
            theta(tg,m)=theta1(tg)+w*N*Tp*(m-1);
            x(tg,m)=radius(tg)*cos(theta(tg,m));
            y(tg,m)=radius(tg)*sin(theta(tg,m));
            if m==1
                range_time(tg,m)=range(tg); %initial range of scatterer before rotation
            else
                range_time(tg,m)=sqrt(a^2+b(tg)^2-2*b(tg)*a*cos(pi-theta(tg,m)) );
                %range of scatterer over time
            end
            %discard last value
            xcoord(tg,m)=center(1)+x(tg,m); %x-co-ordinates of A %diff sign for quad 2
            ycoord(tg,m)=center(2)+y(tg,m); %y-co-ordinates of A
            OA=[xcoord(tg,m)-radarpos(1), ycoord(tg,m)-radarpos(2)]; %vector OA
            RA=[xcoord(tg,m)-center(1), ycoord(tg,m)-center(2)]; %magnitude of RA=radius(tg)
            OAmag(tg,m)= sqrt((xcoord(tg,m)-radarpos(1))^2 + (ycoord(tg,m)-radarpos(2))^2 ); %magnitude of OA
            %angle bet dot product of vectors OA & RA
            beta(tg,m)=acos( dot(OA,RA)/(OAmag(tg,m)*RAmag(tg)));
            del_theta(tg,m)=abs( pi/2-beta(tg,m) );
            vr(tg,m)=-v(tg)*cos(del_theta(tg,m));
            fd(tg,m)=-2*vr(tg,m)/wave;
        end
    elseif ( ( grad(tg)<grad_ref ) | (( grad(tg)==grad_ref ) & (range(tg)<range_ref)) ) %quadrant 2

        for m=1:M
            theta(tg,m)=theta1(tg)-w*N*Tp*(m-1);
            x(tg,m)=radius(tg)*cos(theta(tg,m));
            y(tg,m)=radius(tg)*sin(theta(tg,m));
            if m==1
                range_time(tg,m)=range(tg); %initial range of scatterer before rotation
            else
                range_time(tg,m)=sqrt(a^2+b(tg)^2-2*b(tg)*a*cos(pi-theta(tg,m)) ); %range of scatterer over time
            end

            %Discard last value
            xcoord(tg,m)=center(1)+x(tg,m); %x-co-ordinates of A %diff sign for quad 2
            ycoord(tg,m)=center(2)-y(tg,m); %y-co-ordinates of A %diff in sign
        end
    end
end

```

```

OA=[xcoord(tg,m)-radarpos(1), ycoord(tg,m)-radarpos(2)]; %vector OA
RA=[xcoord(tg,m)-center(1),ycoord(tg,m)-center(2)]; %magnitude of RA=radius(tg)
OAmag(tg,m)= sqrt((xcoord(tg,m)-radarpos(1))^2 + (ycoord(tg,m)-radarpos(2))^2 );
%magnitude of OA
beta(tg,m)=acos( dot(OA,RA)/(OAmag(tg,m)*RAmag(tg) ) );
%angle bet dot product of vectors OA & RA
del_theta(tg,m)=abs( pi/2-beta(tg,m));
vr(tg,m)=v(tg)*cos(del_theta(tg,m));
fd(tg,m)=-2*vr(tg,m)/wave;
    end

elseif( (grad(tg)==grad_ref) & range(tg)==range_ref ) %scatterer is at center
    for m=1:M
        theta(tg,m)=pi;
        x(tg,m)=radius(tg)*cos(theta(tg,m));
        y(tg,m)=radius(tg)*sin(theta(tg,m));
        if m==1
            range_time(tg,m)=range(tg); %initial range of scatterer before rotation
        else
            range_time(tg,m)=sqrt(a^2+b(tg)^2-2*b(tg)*a*cos(pi-theta(tg,m)) );
            %range of scatterer over time
        end
    end
end

end
end

ANS=[fd,vr,range_time(:,1:M)];

%%%%%%%%%%

```

PAGE INTENTIONALLY LEFT BLANK

LIST OF REFERENCES

- [1] Ma Y. B., *Velocity Compensation in Stepped Frequency Radar*, Master's Thesis, Naval Postgraduate School, Monterey, California, December 1995.
- [2] Abraham Thomas Paulose, *High Range Resolution With The Stepped Frequency Waveform*, Master's Thesis, Naval Postgraduate School, Monterey, California, June 1994.
- [3] Victor C. Chen, *Applications of Time-Frequency Processing to Radar Imaging*, Optical Engineering Report, Vol 36 No. 4, Naval Research Laboratory, April 1997.
- [4] James A. Scheer, and James L. Kurtz, *Coherent Radar Performance Estimation*, Artech House Publishers, Boston-London, 1993.
- [5] Donald R. Wehner, *High-Resolution Radar*, Second Edition, Artech House, Inc., Boston-London, 1995.
- [6] Shie Qian, and Dapang Chen, *Joint Time Frequency Analysis*, Prentice hall Inc., New Jersey-USA, 1996.

PAGE INTENTIONALLY LEFT BLANK

INITIAL DISTRIBUTION LIST

1. Defense Technical Information Center.....2
8725 John H. Kingman Rd., STE 0944
Ft. Belvoir, Virginia 22060-6218
2. Dudley Knox Library.....2
Naval Postgraduate School
411 Dyer Rd.
Monterey, California 93943-5000
3. Chairman, Code EC.....1
Department of Electrical and Computer Engineering
Naval Postgraduate School
Monterey, California 93943-5121
4. Professor David C. Jenn, Code EC/Jn.....2
Department of Electrical and Computer Engineering
Naval Postgraduate School
Monterey, California 93943-5121
5. Professor Jefferey B. Knorr, Code EC/Ko.....2
Department of Electrical and Computer Engineering
Naval Postgraduate School
Monterey, California 93943-5121
6. Mun, Kok Leong1
Naval Logistics Department, HQ-RSN
AFPN 6053, 303 Gombak Drive #02-03
Singapore 669645
Singapore
7. Head Librarian1
Defence Technology Tower Library
1 Depot Road, #02-01
Defence Technology Tower A
Singapore 109681
Singapore